Non-oscillatory Central Differencing
for Hyperbolic Conservation Laws

HAIM NESSYAHU AND EITAN TADMOR*

*School of Mathematical Sciences,
Raymond and Beverley Sackler Faculty of Exact Sciences, Tel Aviv University,
Tel Aviv, Israel and
Institute for Computer Applications in Science and Engineering,
NASA Langley Research Center, Hampton, Virginia*

Many of the recently developed high-resolution schemes for hyperbolic conservation laws are based on upwind differencing. The building block of these schemes is the averaging of an approximate Godunov solver; its time consuming part involves the field-by-field decomposition which is required in order to identify the "direction of the wind." Instead, we propose to use as a building block the more robust Lax–Friedrichs (LxF) solver. The main advantage is simplicity: no Riemann problems are solved and hence field-by-field decompositions are avoided. The main disadvantage is the excessive numerical viscosity typical to the LxF solver. We compensate for it by using high-resolution MUSCL-type interpolants. Numerical experiments show that the quality of the results obtained by such convenient central differencing is comparable with those of the upwind schemes. © 1990 Academic Press, Inc.

INTRODUCTION

In this paper we present a family of non-oscillatory, second-order, central difference approximations to non-linear systems of hyperbolic conservation laws. These approximations can be viewed as natural extensions of the first-order Lax–Friedrichs (LxF) scheme. In particular, total-variation and entropy estimates are provided in the scalar case, and unlike the upwind framework, no Riemann problems need to be solved in the case of systems of conservation laws. The use of second-order piecewise-linear approximants instead of the first-order piecewise-constant ones, compensates for the excessive LxF viscosity, and results in second-order resolution Riemann-solver-free family of central difference schemes.

The paper is organized as follows. In Section 2, we derive our family of high resolution central differencing schemes, using the LxF solver together with MUSCL-type interpolants. Thus, at each time-level we reconstruct from the

piecewise constant numerical data, a nonoscillatory piecewise linear approximation of second-order accuracy. We then follow the evolving solution to the next time level and end up by projecting it back to a piecewise constant solution. The result is a family of schemes which takes an easily implemented predictor-corrector form. The resolution of our method hinges upon the choice of certain local *numerical derivatives* with which one reconstructs the piecewise-linear MUSCL-type interpolants from the piecewise-constant data.

In Section 3, we concentrate on the scalar conservation law. We discuss a variety of choices for numerical derivatives and prove that the resulting scalar family of schemes, under the appropriate CFL limitation, satisfies both the total variation diminishing (TVD) property and a cell entropy inequality. These properties guarantee the convergence to the unique entropy solution, at least in the genuinely non-linear scalar case.

In Section 4, we describe several ways to extend our scalar family of central differencing schemes to systems of conservation laws. The main issue lies again in the choice of vectors of numerical derivatives. First, we describe a component-wise extension for the definition of these vectors, which share the simplicity of the scalar family of schemes. Next, we demonstrate the flexibility of our central differencing framework, which enables us to incorporate characteristic information, whenever available, into the definition of numerical derivatives. We continue, by using this characteristic-wise framework to isolate the contact wave where the artificial compression method (ACM) is employed, while treating the more robust sound waves using the less expensive component-wise approach. We end up by presenting a corrective type ACM, which is implemented in a component-wise manner. This both improves the contact resolution and retains the simplicity of the Riemann-solver-free scalar approach.

Finally, in Section 5 we present numerical experiments with our high-resolution non-oscillatory central difference schemes and compare the results with the corresponding upwind-based ones.

Both the quantitative and qualitative results for a representative sample of compressible flow problems governed by the Euler equations, are found to be in complete agreement with the resolution expected by the scalar analysis. Taking into account the ease of implementation, robustness, and time performance, these results compare favorably with the results obtained by the corresponding upwind-based schemes.

2. A FAMILY OF HIGH-RESOLUTION CENTRAL DIFFERENCING METHODS

Many of the recently developed high-resolution schemes, which approximate the one-dimensional system of conservation laws

$$\frac{\partial u}{\partial t} + \frac{\partial}{\partial x}(f(u)) = 0, \tag{2.1}$$

are based on *upwind* differencing. The prototype of such upwind approximations is the Godunov scheme [4]; it computes a piecewise constant approximate solution over cells of width $\Delta x = x_{j+1/2} - x_{j-1/2}$, which is of the form,

$$\bar{v}(x, t) = v_j(t), \qquad x_{j-1/2} \leqslant x < x_{j+1/2}. \tag{2.2}$$

To proceed in time, the Godunov scheme first evolves the piecewise constant solution, $\bar{v}(x, t)$, for a sufficiently small time step Δt. Initiated with $\bar{v}(x, t)$, Eq. (2.1) consists of a successive sequence of non-interacting Riemann problems. Their resulting solution at time level $t + \Delta t$, can be expressed in terms of the Riemann solver, $R(x/t; w_l, w_r)$,

$$v(x, t + \Delta t) = R\left(\frac{x - x_{j+1/2}}{\Delta t}; v_j(t), v_{j+1}(t)\right), \qquad x_j \leqslant x < x_{j+1}. \tag{2.3}$$

This solution is then projected back into the space of piecewise constant gridfunctions, see Fig. 2.1,

$$v_j(t + \Delta t) \equiv \bar{v}(x, t + \Delta t) = \frac{1}{\Delta x} \int_{x_{j-1/2}}^{x_{j+1/2}} v(y, t + \Delta t) \, dy, \qquad x_{j-1/2} \leqslant x < x_{j+1/2}. \tag{2.4}$$

Integration of (2.1) over a typical cell $[x_{j-1/2}, x_{j+1/2}] \times [t, t + \Delta t]$ yields

$$v_j(t + \Delta t) = v_j(t)$$
$$+ \lambda [f(R(0^+; v_{j-1}(t), v_j(t)) - f(R(0^+; v_j(t), v_{j+1}(t)))], \quad \lambda \equiv \Delta t/\Delta x. \tag{2.5}$$
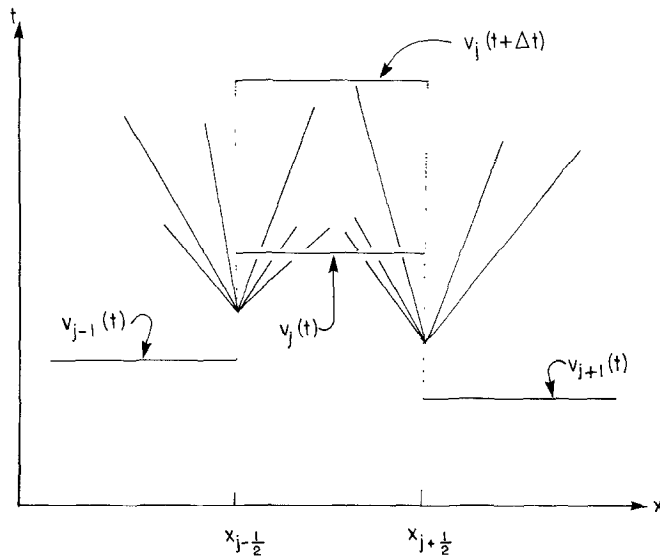

FIGURE 2.1

This shows the upwind property of the Godunov scheme. Namely, if the characteristic speeds throughout the relevant neighbouring cells, $[x_{j-1}, x_{j+1}]$, are all positive (resp. negative), then (2.5) is simplified into $v_j(t + \Delta t) = v_j(t) - \lambda[f(v_j(t)) - f(v_{j-1}(t))]$ (resp. $v_j(t + \Delta t) = v_j(t) - \lambda[f(v_{j+1}(t)) - f(v_j(t))]$). However, a more complex situation occurs when there is a mixture of both rightgoing and leftgoing waves. In this case, the computation of Godunov's numerical flux in (2.5) requires us to identify the "direction of the wind," i.e., to distinguish between the left- and rightgoing waves inside the Riemann fan. The exact (or approximate) solution of the Riemann fan may be an intricate task, and in this context, we mention the field-by-field decomposition proposed by Roe [19], which intends to simplify this task.

Instead, in this section we propose a high resolution approximation of (2.1), which is based on the staggered form of the Lax–Friedrichs (LxF) scheme,

$$v_{j+1/2}(t + \Delta t) = \tfrac{1}{2}[v_j + v_{j+1}] - \lambda[f(v_{j+1}(t)) - f(v_j(t))]. \tag{2.6}$$

The LxF scheme, [13], is a prototype of a central difference approximation, which offers a great simplicity over the upwind Godunov scheme (2.5). We observe that (2.6) can also be interpreted as a piecewise constant projection of successive non-interacting Riemann problems, which are integrated over a staggered grid, see Fig. 2.2,

$$v_{j+1/2}(t + \Delta t) \equiv \bar{v}(x, t + \Delta t)$$

$$= \frac{1}{\Delta x} \int_{x_j}^{x_{j+1}} R\left(\frac{x - x_{j+1/2}}{\Delta t}; v_j, v_{j+1}\right) dx, \qquad x_j \leqslant x < x_{j+1}. \tag{2.7}$$
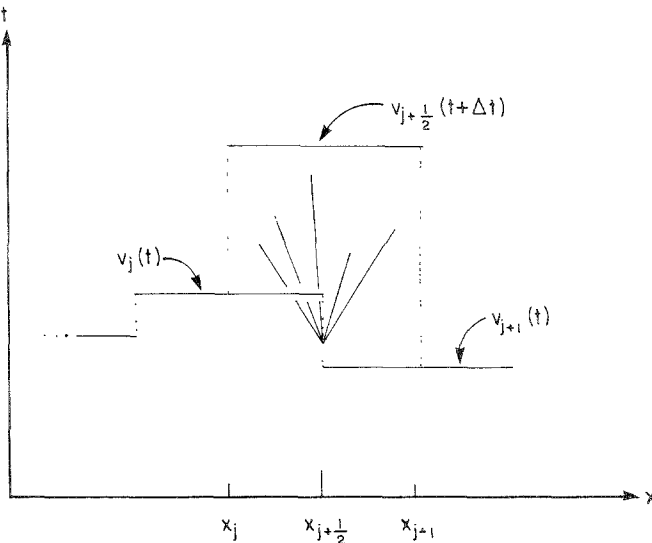

FIGURE 2.2

The robustness of the LxF scheme, (2.7), stems from the fact that unlike the Godunov case, here we integrate over the entire Riemann fan, taking into account both the left- and rightgoing waves. This enables us to ignore any detailed knowledge about the exact (or approximate) Riemann solver $R(\cdot; \cdot, \cdot)$. Unfortunately, the LxF staggered solver, (2.7), which results in the simple recipe (2.6), suffers from excessive numerical viscosity, which is evident from the viscous form [23] $\Delta v_{j+1/2}(t) \equiv v_{j+1}(t) - v_j(t)$

$$v_j(t + \Delta t) = v_j(t) - \tfrac{1}{2}\lambda[f(v_{j+1}(t)) - f(v_{j-1}(t))]$$
$$+ \tfrac{1}{2}[Q_{j+1/2}\Delta v_{j+1/2}(t) - Q_{j-1/2}\Delta v_{j-1/2}(t)]. \tag{2.8}$$

Indeed, the class of upwind schemes is characterized by a numerical viscosity coefficient matrix $Q^U_{j+1/2} \sim \lambda |\bar{A}_{j+1/2}|$, (here $\bar{A}_{j+1/2}$ refers to an approximate average of the Jacobian of $f(v(x, t))$ over the cell $[x_j, x_{j+1}] \times [t, t + \Delta t]$, e.g., [22]). By the CFL limitation, this amount of numerical viscosity is always less than the amount of numerical viscosity present in the central LxF scheme, whose non-staggered form corresponds to $Q^{\mathrm{LxF}} \equiv I$. Consequently, the upwind Godunov-like approximations have better resolution than the central LxF approximation, though they both belong to the same class of first-order accurate schemes. This is one of the main motivations for using upwind schemes as building blocks for the modern shock capturing methods of higher (than first-order) resolution, e.g., [7, 17, 24].

Alternatively, our proposed method will use the simpler central LxF solver as the building block for a family of high-resolution schemes. In this manner we shall retain the LxF main advantage of simplicity: no Riemann problems are solved and hence field-by-field decompositions are avoided. The main disadvantage of excessive numerical viscosity will be compensated by using high-resolution MUSCL interpolants, [24], instead of the first-order piecewise constant ones in (2.2).

To this end, at each time level we first reconstruct from (2.2) a piecewise linear approximation of the form

$$L_j(x, t) = v_j(t) + (x - x_j)\frac{1}{\Delta x}v_j', \qquad x_{j-1/2} \leqslant x < x_{j+1/2}. \tag{2.9a}$$

This form retains conservation, i.e. (here the overbar denotes the $[x_j, x_{j+1}]$-cell average),

$$\bar{L}_j(x, t) = \bar{v}(x, t) = v_j(t);$$

second-order accuracy is guaranteed if the so-called vector of numerical derivative, $(1/\Delta x) v_j'$, which is yet to be determined, satisfies

$$\frac{1}{\Delta x}v_j' = \frac{\partial}{\partial x}v(x = x_j, t) + O(\Delta x). \tag{2.9b}$$

Next, we continue with a second stage, similar to the construction of the central LxF recipe: we evolve the piecewise linear interpolant, (2.9), which is governed by the solution of successive sequences of noninteracting generalized Riemann (GR) problems, [1], see Fig. 2.3,

$$v(x, t + \Delta t) = \text{GR}(x, t + \Delta t; L_j(x, t), L_{j+1}(x, t)), \qquad x_j \leqslant x < x_{j+1}.$$

Finally, the resulting solution is projected back into the space of staggered piecewise-constant gridfunctions

$$v_{j+1/2}(t + \Delta t) = \bar{v}(x, t + \Delta t) \equiv \frac{1}{\Delta x} \int_{x_j}^{x_{j+1}} v(y, t + \Delta t) \, dy, \qquad x_j \leqslant x < x_{j+1}. \quad (2.10)$$

In view of the conservation law (2.1), the last integral equals

$$v_{j+1/2}(t + \Delta t) = \frac{1}{\Delta x} \left[\int_{x_j}^{x_{j+1/2}} L_j(x, t) \, dx + \int_{x_{j+1/2}}^{x_{j+1}} L_{j+1}(x, t) \, dx \right]$$

$$- \frac{1}{\Delta x} \left[\int_{\tau=t}^{t+\Delta t} f(v(x_{j+1}, \tau)) \, d\tau - \int_{\tau=t}^{t+\Delta t} f(v(x_j, \tau)) \, d\tau \right]. \quad (2.11)$$

The first two linear integrands on the right of (2.11), $L_j(x, t)$ and $L_{j+1}(x, t)$, are given by (2.9a) and can be integrated exactly. Moreover, if the CFL condition

$$\lambda \cdot \max_{x_j \leqslant x \leqslant x_{j+1}} \rho(A(v(x, t))) < \tfrac{1}{2} \quad (2.12)$$

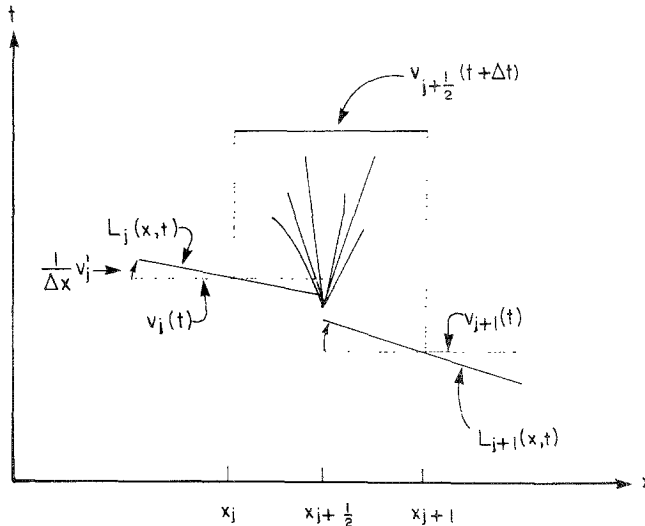FIGURE 2.3

is met, then the last two integrands on the right of (2.11), $f(v(x_j, \tau))$ and $f(v(x_{j+1}, \tau))$, are smooth functions of τ; hence they can be integrated approximately by the midpoint rule at the expense of $O(\Delta t)^3$ local truncation error. Thus we arrive at

$$v_{j+1/2}(t + \Delta t) = \frac{1}{2} \left[v_j(t) + v_{j+1}(t) \right] + \frac{1}{8} \left[v'_j - v'_{j+1} \right]$$

$$- \lambda \left[f\left(v\left(x_{j+1}, t + \frac{\Delta t}{2} \right) \right) - f\left(v\left(x_j, t + \frac{\Delta t}{2} \right) \right) \right]. \quad (2.13)$$

By Taylor expansion and the conservation law (2.1),

$$v\left(x_j, t + \frac{\Delta t}{2} \right) = v_j(t) - \frac{1}{2} \lambda f'_j, \quad (2.14)$$

may serve as our approximate midvalue, $v(x_j, t + \Delta t/2)$, within the permissible second-order accuracy requirement. Here, $(1/\Delta x) f'_j$ stands for an approximate numerical derivative of the flux $f(v(x = x_j, t))$,

$$\frac{1}{\Delta x} f'_j = \frac{\partial}{\partial x} f(v(x = x_j, t)) + O(\Delta x), \quad (2.15)$$

which is yet to be specified.

We should emphasize that while using the central type LxF solver, we integrated over the entire Riemann fan, see $v(x, t + \Delta t)$ in (2.10), which consists of both the left- and rightgoing waves. On the one hand, this enabled us to ignore any detailed knowledge about the exact (or approximate) generalized Riemann solver $GR(\cdot; \cdot, \cdot)$; on the other hand, this enables us to accurately compute the numerical flux, $\int_{\tau=t}^{t+\Delta t} f(v(x, \tau)) \, d\tau$, whose values are extracted from the *smooth* interface of two non-interacting Riemann problems.

In summary, our family of central differencing schemes takes the easily implemented predictor-corrector form,

$$v_j\left(t + \frac{\Delta t}{2} \right) = v_j(t) - \frac{1}{2} \lambda f'_j, \quad (2.16a)$$

$$v_{j+1/2}(t + \Delta t) = \frac{1}{2} \left[v_j(t) + v_{j+1}(t) \right] + \frac{1}{8} \left[v'_j - v'_{j+1} \right]$$

$$- \lambda \left[f\left(v_{j+1}\left(t + \frac{\Delta t}{2} \right) \right) - f\left(v_j\left(t + \frac{\Delta t}{2} \right) \right) \right]. \quad (2.16b)$$

Here the numerical derivatives of both gridfunctions, $\{v_j\}$ and $\{f_j\}$, should obey the accuracy constraints (2.9b) and (2.15). In this manner the second-order accurate corrector step (2.16b) augments the first-order accurate predictor step

(2.16a) and results in a high-resolution second-order central difference approximation of (2.1).

Remarks. 1. The choice $(1/\Delta x)\, v_j' \equiv (1/\Delta x)\, f_j' \equiv 0$ in (2.16), recovers the original first-order accurate LxF scheme (2.6).

2. If instead of (2.6) we use the non-staggered version of the LxF scheme,

$$v_j(t + \Delta t) = \frac{1}{2}\left[v_{j+1}(t) + v_{j-1}(t)\right] - \frac{\lambda}{2}\left[f(v_{j+1}(t)) - f(v_{j-1}(t))\right], \qquad (2.17)$$

and repeat the reconstruction, evolution, and projection steps described above, then the resulting high resolution central differencing approximation amounts to

$$v_j\left(t + \frac{\Delta t}{2}\right) = v_j(t) - \frac{1}{2}\,\lambda f_j', \qquad (2.18a)$$

$$v_j(t + \Delta t) = \frac{1}{2}\left[v_{j+1}(t) + v_{j-1}(t)\right] + \frac{1}{4}\left[v_{j-1}' - v_{j+1}'\right]$$

$$- \frac{\lambda}{2}\left[f\left(v_{j+1}\left(t + \frac{\Delta t}{2}\right)\right) - f\left(v_{j-1}\left(t + \frac{\Delta t}{2}\right)\right)\right]. \qquad (2.18b)$$

To guarantee the desired nonoscillatory property of these approximations, the two free ingredients at our disposal, the numerical derivatives $(1/\Delta x)\, v_j'$ and $(1/\Delta x)\, f_j'$, should be carefully chosen. This issue will be discussed in the next two sections.

3. The Scalar Problem

In this section, we are concerned with non-oscillatory high-resolution central differencing approximations of the scalar conservation law

$$\frac{\partial u}{\partial t} + \frac{\partial}{\partial x}(f(u)) = 0. \qquad (3.1)$$

Our family of high-resolution central differencing schemes (2.16) can be rewritten in the form

$$v_{j+1/2}(t + \Delta t) = \frac{1}{2}\left[v_j(t) + v_{j+1}(t)\right] - \lambda[g_{j+1} - g_j], \qquad (3.2a)$$

where the so-called modified numerical flux, g_j [18], is given by

$$g_j = f\left(v_j\left(t + \frac{\Delta t}{2}\right)\right) + \frac{1}{8\lambda}\, v_j', \qquad v_j\left(t + \frac{\Delta t}{2}\right) = v_j(t) - \frac{1}{2}\,\lambda f_j'. \qquad (3.2b)$$

Here, $(1/\Delta x) v_j'$ is an approximate slope at the grid point x_j,

$$\frac{1}{\Delta x} v_j' = \frac{\partial}{\partial x} v(x = x_j, t) + O(\Delta x), \tag{3.3a}$$

and $(1/\Delta x) f_j'$ is the numerical derivative of the gridfunction $\{f_j\}$,

$$\frac{1}{\Delta x} f_j' = \frac{\partial}{\partial x} f(v(x = x_j, t)) + O(\Delta x). \tag{3.3b}$$

The constraints (3.3) with smooth (= Lipschitz continuous) first-order perturbations on their right, guarantee the second-order accuracy of the central differencing schemes (3.2). In order to ensure that these schemes are also non-oscillatory in the sense to be described below, our numerical derivatives, $(1/\Delta x) w_j'$, should satisfy for every gridfunction $w = \{w_j\}$,

$$0 \leqslant w_j' \cdot \mathrm{sgn}(\Delta w_{j \pm 1/2}) \leqslant \mathrm{Const} \cdot |\mathrm{Min\ Mod}\{\Delta w_{j+1/2}, \Delta w_{j-1/2}\}|. \tag{3.4a}$$

Here, the Min Mod$\{\cdot, \cdot\}$ stands for the usual limiter,

$$\mathrm{MM}\{x, y\} \equiv \mathrm{Min\ Mod}\{x, y\} = \tfrac{1}{2}\left[\mathrm{sgn}(x) + \mathrm{sgn}(y)\right] \cdot \mathrm{Min}(|x|, |y|), \tag{3.4b}$$

and can be similarly extended to include more (than two) variables. The constraint (3.4) is required in order to guarantee the total variation dimishing (TVD) property for the family of central differencing schemes (3.2). We recall that TVD is a desirable property in the current setup, for it implies no spurious oscillations in our approximate solution $v(x, t)$ [7].

However, it is well known, e.g., [7, 18], that one cannot satisfy both the accuracy requirement, (3.3), and the TVD requirement, (3.4), at the non-sonic critical gridvalues, v_j, where $\Delta v_{j+1/2} \cdot \Delta v_{j-1/2} < 0 \neq a(v_j)$, $a(v_j) \equiv df(v)/dv_{|v=v_j}$. Therefore, the second-order accuracy requirement, (3.3), must be given up at these critical gridvalues. Difference schemes with (formal) second-order accuracy at all but these critical grid values may be classified as having second-order resolution in the sense that the local truncation error is almost everywhere $O(\Delta x)^3$, and the overall second-order accuracy does not seem to be degraded in such cases, at least in the L^1-norm. We shall verify the TVD property of the central differencing schemes, (3.2), with the help of

LEMMA 3.1. *The scheme (3.2a) is TVD, if its modified numerical flux, g_j, satisfies the following generalized CFL condition,*

$$\lambda \left| \frac{\Delta g_{j+1/2}}{\Delta v_{j+1/2}} \right| \leqslant \frac{1}{2}, \qquad \Delta g_{j+1/2} \equiv g_{j+1} - g_j. \tag{3.5}$$

Indeed, by (3.2a), the difference $v_{j+1/2}(t+\Delta t) - v_{j-1/2}(t+\Delta t)$ equals

$$v_{j+1/2}(t+\Delta t) - v_{j-1/2}(t+\Delta t)$$
$$= \Delta v_{j+1/2}\left(\frac{1}{2} - \lambda\frac{\Delta g_{j+1/2}}{\Delta v_{j+1/2}}\right) + \Delta v_{j-1/2}\left(\frac{1}{2} + \lambda\frac{\Delta g_{j-1/2}}{\Delta v_{j-1/2}}\right).$$

Condition (3.5) tells us that the terms inside the parenthesis are positive and TVD follows along the lines of [7],

$$TV(v(t+\Delta t)) \equiv \sum_j |v_{j+1/2}(t+\Delta t) - v_{j-1/2}(t+\Delta t)| \leqslant TV(v(t)). \tag{3.6}$$

Equipped with Lemma 3.1 we turn to

THEOREM 3.2. *Let the numerical derivatives $(1/\Delta x)v_j'$ and $(1/\Delta x)f_j'$ in (3.3) be chosen such that the TVD requirement (3.4) holds, say,*

$$0 \leqslant v_j' \cdot \mathrm{sgn}(\Delta v_{j\pm 1/2}) \leqslant \mathrm{Const}_v \cdot |\mathrm{MM}\{\Delta v_{j+1/2}, \Delta v_{j-1/2}\}|, \qquad \mathrm{Const}_v \equiv \alpha, \tag{3.7a}$$

$$0 \leqslant f_j' \cdot \mathrm{sgn}(\Delta v_{j\pm 1/2}) \leqslant \mathrm{Const}_f \cdot |\mathrm{MM}\{\Delta v_{j+1/2}, \Delta v_{j-1/2}\}|. \tag{3.7b}$$

Assume that the following CFL condition is satisfied

$$\lambda \cdot \max_j |a(v_j)| \leqslant \beta, \qquad \beta \equiv \lambda\frac{\mathrm{Const}_f}{\mathrm{Const}_v} \leqslant \frac{1}{2\alpha}(\sqrt{4+4\alpha-\alpha^2}-2). \tag{3.8}$$

Then the family of high-resolution central differencing schemes (3.2), (3.3) is TVD.

Proof. By (3.2b) we have:

$$\lambda\left|\frac{\Delta g_{j+1/2}}{\Delta v_{j+1/2}}\right| \leqslant \lambda\left|\frac{f(v_{j+1}(t+\Delta t/2)) - f(v_j(t+\Delta t/2))}{\Delta v_{j+1/2}}\right| + \frac{1}{8}\cdot\left|\frac{\Delta v_{j+1/2}'}{\Delta v_{j+1/2}}\right|$$
$$\leqslant \lambda\left|\frac{f(v_{j+1}(t+\Delta t/2)) - f(v_j(t+\Delta t/2))}{v_{j+1}(t+\Delta t/2) - v_j(t+\Delta t/2)}\right| \cdot \left|\frac{v_{j+1}(t+\Delta t/2) - v_j(t+\Delta t/2)}{\Delta v_{j+1/2}}\right|$$
$$+ \frac{1}{8}\left|\frac{\Delta v_{j+1/2}'}{\Delta v_{j+1/2}}\right|. \tag{3.9}$$

Our CFL condition (3.8) implies that the first term on the right of (3.9) does not exceed

$$\lambda\left|\frac{f(v_{j+1}(t+\Delta t/2)) - f(v_j(t+\Delta t/2))}{v_{j+1}(t+\Delta t/2) - v_j(t+\Delta t/2)}\right| \leqslant \beta. \tag{3.10}$$

Using the midvalue $v_j(t+\Delta t/2)$ in (3.2b), we can estimate the second term on the right of (3.9),

$$\left|\frac{v_{j+1}(t+\Delta t/2) - v_j(t+\Delta t/2)}{\Delta v_{j+1/2}}\right| \leqslant 1 + \frac{\lambda}{2}\left|\frac{\Delta f_{j+1/2}'}{\Delta v_{j+1/2}}\right|, \qquad \Delta f_{j+1/2}' \equiv f_{j+1}' - f_j', \tag{3.11a}$$

where in view of (3.7b) and (3.8),

$$\left|\frac{\Delta f'_{j+1/2}}{\Delta v_{j+1/2}}\right| \leqslant \max\left(\left|\frac{f'_j}{\Delta v_{j+1/2}}\right|, \left|\frac{f'_{j+1}}{\Delta v_{j+1/2}}\right|\right) \leqslant \text{Const}_f = \frac{1}{\lambda}\alpha\beta. \qquad (3.11b)$$

Finally, the TVD requirement, (3.7a), gives us an upper bound for the third term on the right of (3.9),

$$\left|\frac{\Delta v'_{j+1/2}}{\Delta v_{j+1/2}}\right| \leqslant \max\left(\left|\frac{v'_j}{\Delta v_{j+1/2}}\right|, \left|\frac{v'_{j+1}}{\Delta v_{j+1/2}}\right|\right) \leqslant \alpha. \qquad (3.12)$$

Using (3.10), (3.11), and (3.12), we find that (3.9) boils down to the quadratic inequality

$$\beta(1 + \tfrac{1}{2}\alpha\beta) + \tfrac{1}{8}\alpha \leqslant \tfrac{1}{2},$$

whose solution yields the CFL limitation (3.8).

Remarks. 1. The values α which permit a positive solution of (3.8), $\beta > 0$, are $0 \leqslant \alpha < 4$.

2. The TVD constraints (3.7) with $\alpha = 0$ yields $v'_j \equiv f'_j \equiv 0$, which recovers the staggered LxF scheme (2.6) with the corresponding CFL condition $\beta < \tfrac{1}{2}$.

3. The CFL restriction (3.5) is a sufficient but not necessary condition for the TVD property. In practice one may use higher values of β, up to $\beta \lesssim \tfrac{1}{2}$.

4. A similar analysis carried out for the non-staggered form, (2.18), yields

$$\beta \leqslant \frac{1}{\alpha}(\sqrt{1 + 2\alpha - \alpha^2} - 1)$$

instead of (3.8). In practice one may use $\beta \lesssim 1$ in this case.

We shall now discuss a few examples of numerical derivatives, which retain both the second order resolution constraint, (3.3), and the TVD constraints, (3.7). As our first example for the numerical derivative, v'_j, we choose

$$v'_j = \text{MM}\{\Delta v_{j+1/2}, \Delta v_{j-1/2}\}. \qquad (3.13a)$$

This choice may oversmear a strong "discontinuity," where the order of accuracy is less significant. A preferable second choice, which allows for a steeper slope near such discontinuities and yet retains higher accuracy in smooth regions, is given by

$$v'_j = \text{MM}\{\alpha\Delta v_{j+1/2}, \tfrac{1}{2}(v_{j+1} - v_{j-1}), \alpha\Delta v_{j-1/2}\}. \qquad (3.13b)$$

The limiting parameter α can range between the values $\alpha = 1$, which corresponds to the basic MinMod limiter in (3.13a), and up to $\alpha < 4$, which is permitted by the CFL conditions (3.8). Similarly, the flux numerical derivative may be chosen as

$$f'_j = \text{MM}\{\Delta f_{j+1/2}, \Delta f_{j-1/2}\}, \qquad (3.14a)$$

which is a special case of

$$f'_j = \mathrm{MM}\{\alpha \Delta f_{j+1/2}, \tfrac{1}{2}(f_{j+1} - f_{j-1}), \alpha \Delta f_{j-1/2}\}. \qquad (3.14b)$$

A simpler alternative for (3.14) is given by

$$f'_j = a(v_j)v'_j, \qquad (3.15)$$

where v'_j is already computed by (3.13). We observe that this choice saves half the computation time of the MinMod operation; yet, it requires the computation of the Jacobian, $A(v_j)$, when dealing with systems of conservation laws.

The numerical derivative chosen in (3.13a), (3.14a) satisfies (3.7) with $\alpha = 1$, which implies the TVD property under the CFL limitation (3.8) with $\beta = \tfrac{1}{2}(\sqrt{7} - 2) \approx 0.32$.

The numerical derivative chosen in (3.13b), (3.14b) clearly satisfies (3.7) and consequently the TVD property, for every permissable α, $0 \leqslant \alpha < 4$. We summarize the above by stating

COROLLARY 3.3.   *Let the numerical derivative $(1/\Delta x)\,v'_j$ be chosen by*

$$v'_j = \mathrm{MM}\{\Delta v_{j+1/2}, \Delta v_{j-1/2}\}; \qquad (3.16a)$$

let the flux numerical derivative be chosen either by

$$f'_j = a(v_j)v'_j \qquad (3.16b)$$

or

$$f'_j = \mathrm{MM}\{\Delta f_{j+1/2}, \Delta f_{j-1/2}\}. \qquad (3.16c)$$

Then the family of high resolution central differencing schemes (3.2), (3.16) is TVD under the CFL condition

$$\lambda \cdot \max_j |a(v_j)| \leqslant \beta, \qquad \beta = \tfrac{1}{2}(\sqrt{7} - 2) \approx 0.32.$$

Similarly, we have

COROLLARY 3.4.   *Let the numerical derivative $(1/\Delta x)v'_j$ be chosen by*

$$v'_j = \mathrm{MM}\{2\Delta v_{j+1/2}, \tfrac{1}{2}(v_{j+1} - v_{j-1}), 2\Delta v_{j-1/2}\}; \qquad (3.17a)$$

let the flux numerical derivative be chosen either by

$$f'_j = a(v_j)v'_j \qquad (3.17b)$$

or

$$f'_j = \mathrm{MM}\{2\Delta f_{j+1/2}, \tfrac{1}{2}(f_{j+1} - f_{j-1}), 2\Delta f_{j-1/2}\}. \qquad (3.17c)$$

Then the family of high resolution central differencing schemes (3.2), (3.17) *is TVD, under the CFL condition,*

$$\lambda \cdot \max_j |a(v_j)| \leqslant \beta, \qquad \beta = \tfrac{1}{2}(\sqrt{2} - 1) \approx 0.21.$$

Remarks. 1. We note that the CFL limitations in Corollaries 3.3 and 3.4 are not sharp. In the first case, (3.16), where a limiter parameter $\alpha = 1$ was used, the reconstruction step is a TVD operation; replacing the exact TVD evolution operator by the midpoint rule in (2.11) together with the final averaging step is also TVD, under the CFL limitation $\beta \leqslant \tfrac{1}{2}$. Similarly, one can argue that in the second case, (3.17), where a limiter parameter $\alpha = 2$ was used, the averaging step retains the TVD property (though not necessarily the entropy condition), as long as the CFL condition $\beta \leqslant \tfrac{1}{2}$ is met. Indeed, this CFL condition was verified as the stability limitation, by the numerical experiments reported in Section 5.

2. Recently, non-oscillatory schemes were constructed, such that by sacrificing the TVD property, they achieve higher (than second-order) resolution including the critical grid-values, e.g., the UNO scheme in [12] and the ENO class of approximations in [9]. To implement such ideas within our framework, one can borrow their definition of numerical derivative. For example, instead of the TVD choices (3.4), our central differencing scheme (3.2) may be augmented by the UNO choice (here $\Delta^2 v_j \equiv v_{j+1} - 2v_j + v_{j-1}$),

$$v'_j = \text{MM}\{\Delta v_{j-1/2} + \tfrac{1}{2}\,\text{MM}(\Delta^2 v_{j-1}, \Delta^2 v_j), \Delta v_{j+1/2} - \tfrac{1}{2}\,\text{MM}(\Delta^2 v_j, \Delta^2 v_{j+1})\}. \qquad (3.18)$$

Theorem 3.2 and its corollaries 3.3 and 3.4 demonstrate high-resolution central differencing methods which satisfy the non-oscillatory TVD property, and hence are convergent to a limit solution $u(x, t)$. To guarantee that this limit solution is the unique entropy solution of the scalar conservation law (3.1), we shall appeal to the following cell entropy inequality, see [10],

$$U(v_{j+1/2}(t + \Delta t)) \leqslant \tfrac{1}{2} [U(v_j) + U(v_{j+1})] - \lambda [G_{j+1} - G_j]. \qquad (3.19)$$

Here $U(u)$ is a convex entropy function and $G_j \equiv G(v_{j+1}, v_j, v_{j-1})$ is the numerical entropy flux which is consistent with the corresponding differential one

$$G(u, u, u) = F(u), \qquad F(u) \equiv \int^u f'(u)\,U'(u).$$

We recall that Lax has verified such cell entropy inequality for the LxF scheme, [14]. Following Lax, we will continuously deform v_j into v_{j+1},

$$v(s) = sv_j + (1 - s)\,v_{j+1}, \qquad v(0) = v_{j+1}, v(1) = v_j, \qquad (3.20a)$$

and, in a similar manner we will further deform $v(s)$ into v_{j+1},

$$v(r, s) = rv(s) + (1 - r)\,v_{j+1}, \qquad v(0, s) = v_{j+1}, v(1, s) = v(s). \qquad (3.20b)$$

In the Appendix we prove

LEMMA 3.5. *Let $g(v)$ be a piecewise differentiable interpolant of the gridfunction $\{g_j\}$. Then the following identity holds,*

$$U(v_{j+1/2}(t+\Delta t)) \equiv \tfrac{1}{2} \left[U(v_{j+1} + U(v_j) \right]$$

$$- \lambda \int_{v_j}^{v_{j+1}} U'(v) \ g'(v) \ dv - R_{j+1/2}^U(g(v)). \tag{3.21}$$

Here the residual term, $R_{j+1/2}(g) \equiv R_{j+1/2}^U(g(v))$, is given by,

$$R_{j+1/2}^U(g(v)) = (\Delta v_{j+1/2})^2 \int_0^1 \int_0^1 s U''(v(r,s))$$

$$\cdot \left[\tfrac{1}{2} - \lambda g'(v(r,s)) \right] \cdot \left[\tfrac{1}{2} + \lambda g'(v(s)) \right] ds \ dr. \tag{3.22}$$

Adding and subtracting

$$\int_{v_j}^{v_{j+1}} U'(u) f'(u) \ du \equiv F(v_{j+1}) - F(v_j),$$

then after integration by parts, the right-hand side of (3.21) will amount to:

$$U(v_{j+1/2}(t+\Delta t)) = \tfrac{1}{2} \left[U(v_{j+1}) + U(v_j) \right]$$

$$- \lambda [F(v_{j+1}) - F(v_j)] - \lambda U'(v) \cdot (g(v) - f(v))|_{v_j}^{v_{j+1}}$$

$$+ \lambda \int_{v_j}^{v_{j+1}} U''(v) \cdot (g(v) - f(v)) \ dv - R_{j+1/2}^U(g(v)).$$

Consequently, the inequality

$$\lambda \int_{v_j}^{v_{j+1}} U''(v) \cdot (g(v) - f(v)) \ dv - R_{j+1/2}^U(g(v)) \leqslant 0 \tag{3.23}$$

provides us with a sufficient condition for the family of central differencing schemes (3.2) to satisfy the cell entropy inequality, (3.19), with numerical entropy flux $G_j = F(v_j) + U'(v_j) \cdot (g(v_j) - f(v_j))$. This brings us to

LEMMA 3.6. *Let $g(v)$ be the piecewise linear interpolant of the modified flux gridfunction $\{g_j\}$,*

$$g(v) = \frac{\Delta g_{j+1/2}}{\Delta v_{j+1/2}} (v - v_j) + g_j, \qquad \min(v_j, v_{j+1}) \leqslant v \leqslant \max(v_j, v_{j+1}). \tag{3.24}$$

Assume that the central differencing schemes (3.2), satisfy the TVD constraint (consult (3.7)),

$$0 \leqslant v_j' \cdot \mathrm{sgn}(\Delta v_{j\pm1/2}) \leqslant \mathrm{Const}_v \cdot |\mathrm{MM}\{\widetilde{\Delta v}_{j+1/2}, \widetilde{\Delta v}_{j-1/2}\}|, \quad \mathrm{Const}_v \equiv \alpha \leqslant 1, \tag{3.25a}$$

where

$$\widetilde{\Delta v}_{j+1/2} \equiv \Delta v_{j+1/2} \cdot [1 - \lambda \cdot (\max_x f''(v(x)) \cdot \Delta v_{j+1/2})^+]^+. \tag{3.25b}$$

The entropy dissipative limiter in (3.25b), *is introduced in order to prevent the nonexpansive entropy violating rarefactions, consult* [18, *Section* 8].

Moreover, assume that the flux numerical derivative satisfies the TVD constraint:

$$0 \leqslant f'_j \cdot \text{sgn}(\Delta v_{j\pm 1/2}) \leqslant \text{Const}_f \cdot |\text{MM}\{\Delta v_{j+1/2}, \Delta v_{j-1/2}\}|, \qquad \lambda \cdot \frac{\text{Const}_f}{\text{Const}_v} \equiv \beta, \tag{3.25c}$$

so that te CFL condition (3.8) *holds. Then the following inequality holds*:

$$\lambda \int_{v_j}^{v_{j+1}} (g(v) - f(v)) \, dv - R^U_{j+1/2}(g(v)) \leqslant 0, \qquad U(u) = \tfrac{1}{2} u^2. \tag{3.26}$$

Remarks.   1.   We observe that in the genuinely non-linear (GNL) case, where, say, $f'' > 0$, the entropy constraint (3.25b) becomes effective only in rarefactions cells where $\Delta v_{j+1/2} > 0$, in agreement with [18]. It retains the second-order resolution of the central differencing schemes (3.2), except for a finite number of critical cells which contain strong rarefactions, $(\Delta v_{j+1/2})^+ \sim 1$, where it reduces (3.2, (3.3) to the original LxF scheme.

2.   Lemma 3.6 applies to choices of numerical derivatives, v'_j, subject to the TVD constraint (3.7a) with $0 < \alpha \leqslant 1$. In practice, higher values, $\alpha > 1$, can be used.

Lemma 3.6, which is proved in the Appendix, shows that our central differencing TVD schemes (3.2), (3.7) fulfill the sufficient condition (3.23) and consequently the cell entropy inequality (3.19), with respect to the quadratic entropy function $U(u) = \tfrac{1}{2} u^2$. Thus, the limit solution of our central TVD schemes, $u(x, t)$, satisfies

$$\frac{\partial}{\partial t}\left(\frac{1}{2} u^2\right) + \frac{\partial}{\partial x}(F(u)) \leqslant 0, \qquad F(u) = \int^u u f'(u) \, du.$$

This singles out $u(x, t)$ as the unique entropy solution of (3.1), at least in the GNL case [2]. We have shown

THEOREM 3.7.   *Consider the GNL scalar conservation law* (3.1). *It is approximated by the family of high resolution central differencing schemes* (3.2), (3.3) *which satisfy the TVD and entropy constraints,* (3.25). *Then, if the CFL condition* (3.8) *holds, we have*:

1.   *second-order resolution*;

2.   *total variation diminishing property*;

3.   *a consistent quadratic cell-entropy inequality*;

and, as a consequence of 2 and 3:

4. *the corresponding central differencing schemes converge to the unique physically relevant solution of the GNL conservation law* (3.1).

We shall close this section with some scalar numerical examples. We consider the approximate solution of the inviscid Burgers' equation

$$u_t + (\tfrac{1}{2} u^2)_x = 0, \tag{3.27}$$

using several of the previously mentioned central differencing schemes. They include:

1. The first-order LxF scheme in its non-staggered form (2.17).

2. The second-order non-oscillatory central differencing scheme (2.18), (3.13a), (3.15). This is the ordinary *non-staggered* version of our central differencing which will be referred to as ORD.

3. The second-order non-oscillatory central differencing scheme (3.2), (3.13a), (3.15). This is the *staggered* version of our central differencing which will be referred to as STG.

Equation (3.27) is solved with two sets of initial conditions. In the first case, we have the smooth 1-periodic initial data,

$$u(x, 0) = \sin(\pi x). \tag{3.28a}$$

The well-known solution of (3.27), (3.28a), e.g., [15], develops a shock discontinuity at $t_c \approx 0.31$. Table I shows us the L_1 norm of the errors at the pre-shock time $t = 0.15$. It indicates the first-order accuracy of the LxF scheme in contrast to the second-order accuracy of our central differencing, ORD and STG. In Table I we also recorded the same L_1 norm of the errors at the post-shock time $t = 0.4$. The presence of a shock discontinuity in this case, reduces the global L_1 error to first order. However, the central differencing STG scheme performs somewhat better than the central differencing ORD scheme and they both have better resolution than the first-order LxF scheme in shock-free zones.

TABLE I

L_1-Norm of the Errors for Numerical Solutions of $u_t + uu_x = 0$, $u(x, 0) = \sin(\pi x)$

	$t = 0.15$			$t = 0.4$		
N	LxF	ORD	STG	LxF	ORD	STG
40	0.023702	0.002620	0.000859	0.044449	0.003612	0.000849
80	0.12249	0.000667	0.000232	0.023486	0.001291	0.000277
160	0.006246	0.000169	0.000061	0.011383	0.000498	0.000098
320	0.003158	0.000043	0.000016	0.005235	0.000209	0.000038
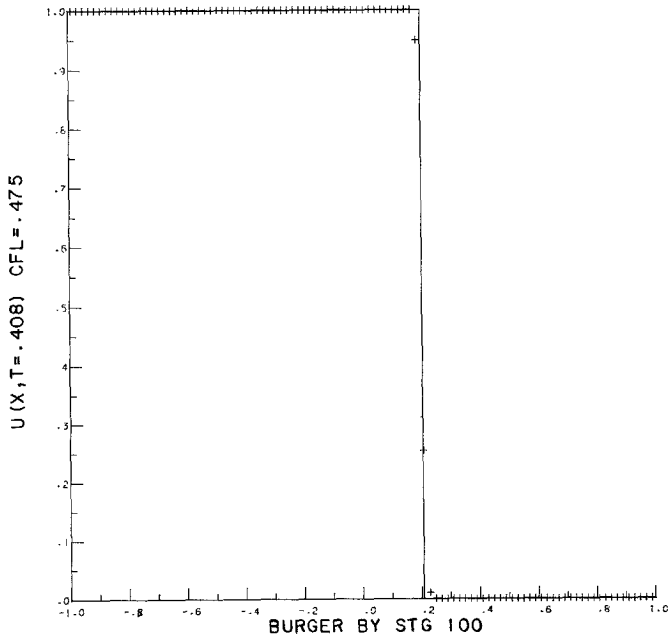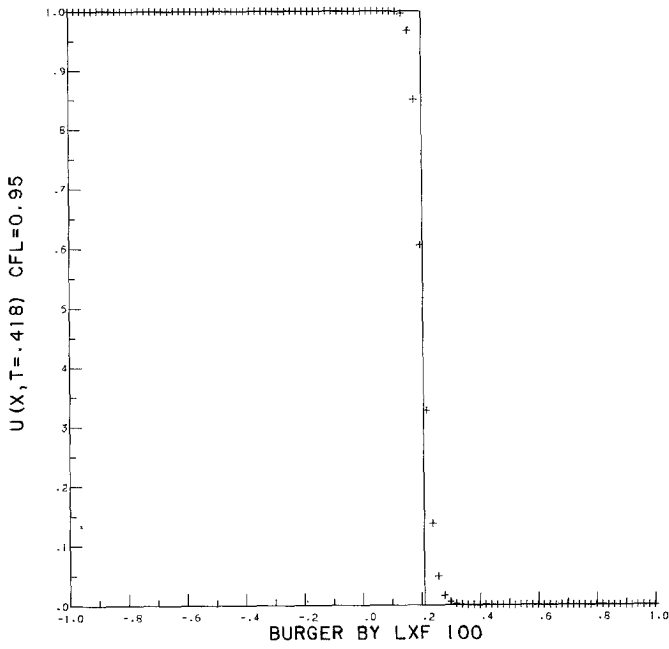
FIGURE 3.1
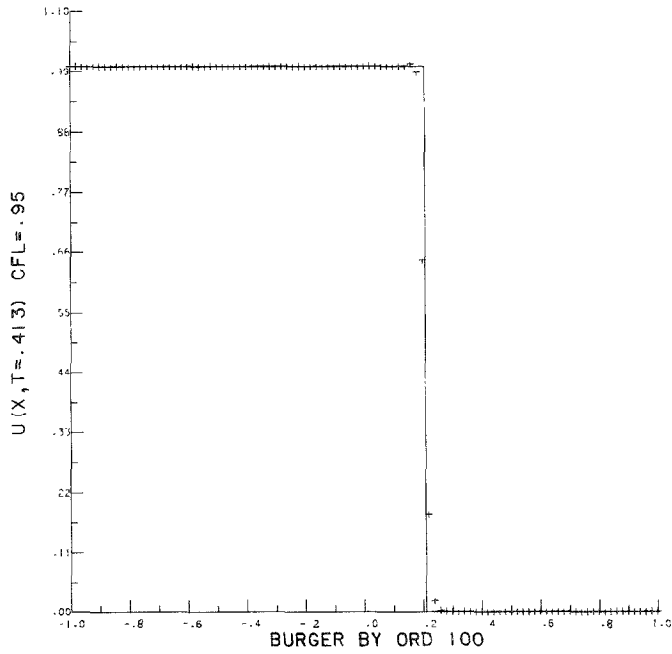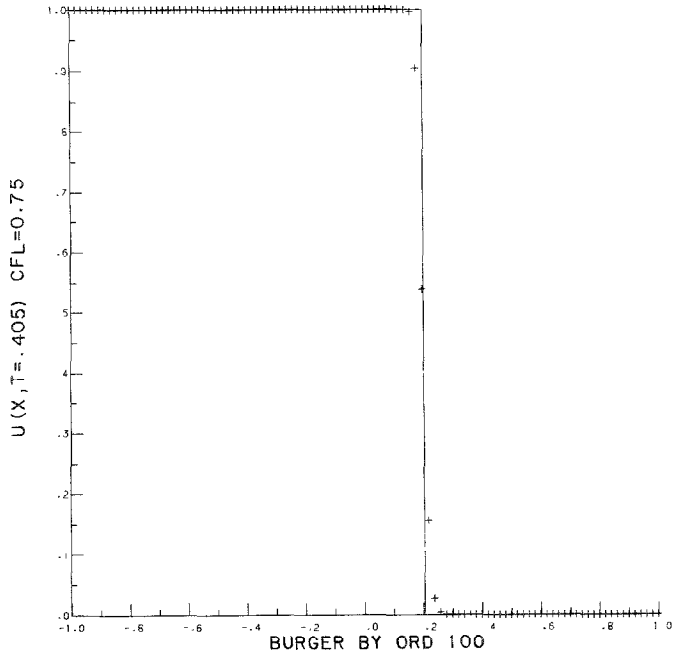
FIG. 3.1—*Continued*

This behavior is amplified in the case of solving Burgers' equation (3.27), with Riemann initial data

$$u(x, 0) = \begin{cases} 1, & x < 0 \\ 0, & x \geqslant 0. \end{cases} \qquad (3.28b)$$

In this case the steady shock solution is resolved by the numerical schemes as a viscous profile shown in Fig. 3.1. Figure 3.1 illustrates the over-smearing of the LxF profile, when compared with those of the ORD and STG schemes. Once more, we observe that the STG scheme has somewhat better resolution than its non-staggered counterpart ORD. Yet, the CFL limitation is the non-staggered form, $\beta \lesssim 1$, results in a better time preformance than the STG scheme which is subject to the CFL limitation $\beta \lesssim \frac{1}{2}$. (We recall that the sufficient TVD constraint in Theorem 3.2 is more restrictive than the usual CFL limitation; indeed, we note that the numerical solution by the ORD version of our scheme is TVD under CFL limitation $\beta \leqslant 0.75$, yet its variation siglhtly increases with $\beta = 0.95$.) In either case, these easily implemented non-oscillatory central differencing outperform the first-order LxF one.

4. SYSTEMS OF CONSERVATION LAWS

In this section, we describe how to extend our family of scalar central differencing schemes to the one-dimensional system of conservation laws,

$$\frac{\partial u}{\partial t} + \frac{\partial}{\partial x} (f(u)) = 0. \qquad (4.1)$$

Here $u(x, t)$ is the unknown N-vector of the form

$$u = (u_1(x, t), u_2(x, t), ..., u_N(x, t))^{\mathrm{T}},$$

and $f(u)$ is the flux vector,

$$f(u) = (f_1(u), f_2(u), ..., f_N(u))^{\mathrm{T}},$$

with an $N \times N$ Jacobian matrix,

$$A_{pq}(u_1, ..., u_N) = \left(\frac{\partial f_p}{\partial u_q}\right), \qquad p, q = 1, ..., N.$$

Our approximate solution at the gridpoint x_j is given by the N-vector,

$$v_j = (v_{j,1}, v_{j,2}, ..., v_{j,N})^{\mathrm{T}},$$

and the corresponding vector of differences, $\Delta v_{j+1/2} = v_{j+1} - v_j$, consists of N-components denoted by $\Delta v_{j+1/2,k} = v_{j+1,k} - v_{j,k}$.

Equipped with these notations, our family of high-resolution central differencing schemes (3.2), (3.3), takes the form,

$$v_{j+1/2}(t+\Delta t) = \tfrac{1}{2}\left[v_j(t)+v_{j+1}(t)\right] - \lambda[g_{j+1}-g_j], \tag{4.2a}$$

where the modified numerical flux, g_j, is given by

$$g_j = f\left(v_j\left(t+\frac{\Delta t}{2}\right)\right) + \frac{1}{8\lambda}v_j', \qquad v_j\left(t+\frac{\Delta t}{2}\right) = v_j(t) - \frac{1}{2}\lambda f_j'. \tag{4.2b}$$

As before, the computation of g_j and $v_j(t+\Delta t/2)$ requires the numerical derivatives of the gridfunctions $\{v_j\}$ and $\{f_j\}$. This time we have to choose two N-vectors of numerical derivatives,

$$\frac{1}{\Delta x}v_j' = (v_{j,1}', v_{j,2}', ..., v_{j,N}')^{\mathrm{T}}, \tag{4.3a}$$

$$\frac{1}{\Delta x}f_j' = (f_{j,1}', f_{j,2}', ..., f_{j,N}')^{\mathrm{T}}. \tag{4.3b}$$

In the rest of this section, we shall describe the pros and cons of several choices for these vectors of numerical derivatives.

Our first choice is a component-wise extension of the scalar definition in Section 3. To this end we may use either (4.4a),

$$v_{j,k}' = \mathrm{MM}\{\Delta v_{j+1/2,k}, \Delta v_{j-1/2,k}\}, \qquad k=1,...,N, \tag{4.4a}$$

or the more general (4.4b),

$$v_{j,k}' = \mathrm{MM}\{\alpha\Delta v_{j+1/2,k}, \tfrac{1}{2}(v_{j+1,k}-v_{j-1,k}), \alpha\Delta v_{j-1/2,k}\}, \qquad k=1,...,N, \tag{4.4b}$$

or instead, use the UNO-like numerical derivative in (3.18),

$$v_{j,k}' = \mathrm{MM}\{\Delta v_{j-1/2,k} + \tfrac{1}{2}\mathrm{MM}(\Delta^2 v_{j-1,k}\Delta^2 v_{j,k}),$$
$$\Delta v_{j+1/2,k} - \tfrac{1}{2}\mathrm{MM}(\Delta^2 v_{j,k}, \Delta^2 v_{j+1,k})\}, \qquad k=1,...,N. \tag{4.4c}$$

A possible choice for the vector of numerical flux derivative may be

$$f_j' = A(v_j)v_j'. \tag{4.5}$$

This approach involves multiplication of the Jacobian matrix by the vector of derivatives, v_j'. This multiplication may be avoided if we use a component-wise definition for the vector of numerical flux derivatives, f_j, in analogy to (3.14). For example, we may use

$$f_{j,k}' = \mathrm{MM}\{\Delta f_{j+1/2,k}, \Delta f_{j-1/2,k}\} \tag{4.6a}$$

or, alternatively,

$$f_{j,k}' = \mathrm{MM}\{\alpha\Delta f_{j+1/2,k}, \tfrac{1}{2}(f_{j+1,k}-f_{j-1,k}), \alpha\Delta f_{j-1/2,k}\}. \tag{4.6b}$$

We observe that the Jacobian free form (JFF), (4.4), (4.6) avoids the use of the Jacobian matrix $A(v)$ required by (4.4), (4.5), at the expense of carrying out the MinMod operation twice.

The resulting central differencing schemes, (4.2), which are based upon the component-wise definition of the numerical derivatives in (4.4)–(4.6), share the simplicity of the scalar framework. Namely, no Riemann problems are solved and consequently characteristic decompositions, required in order to distinguish between the left- and rightgoing waves inside the Riemann fan, are avoided. At the same time, our central differencing approach is flexible enough so that it enables us to incorporate characteristic information, whenever available, in order to achieve improved resolution.

Our next choice shows how to incorporate the characteristic information into the definition of the numerical derivatives. To this end we shall employ a Roe matrix, $\hat{A}_{j+1/2} = A(v_j, v_{j+1})$, namely, an averaged Jacobian, $\hat{A}_{j+1/2}$, satisfying, e.g., [11, 19],

$$f(v_{j+1}) - f(v_j) = \hat{A}_{j+1/2} \cdot (v_{j+1} - v_j), \tag{4.7}$$

and having complete real eigensystem $\{\hat{a}_{j+1/2,k}, \hat{R}_{j+1/2,k}\}, k = 1, ..., N$. Let us project the vector of differences $\Delta v_{j+1/2}$ onto $\{\hat{R}_{j+1/2}\}$; i.e., we use the characteristic decomposition

$$\Delta v_{j+1/2} = \sum_k \hat{\alpha}_{j+1/2,k} \cdot \hat{R}_{j+1/2,k}, \qquad k = 1, ..., N, \tag{4.8a}$$

where

$$\hat{a} \qquad = \hat{\ell} \qquad \Delta v \qquad \hat{\ell} \cdot \hat{R} = \delta \qquad k = 1 \qquad N \qquad (4.8b)$$

Then the corresponding projection of the flux vector of differences is given by

$$\Delta f_{j+1/2} = \sum_k \hat{\alpha}_{j+1/2,k} \hat{a}_{j+1/2,k} \hat{R}_{j+1/2,k}. \tag{4.9}$$

Now, a possible characteristic-wise choice for the numerical derivatives in analogy with (4.4), may be (here $\hat{R}_{j,k}$ is denotes the averaged eigenvector centered at $x = x_j$),

$$v'_{j,k} = \sum_k \text{MM}\{\hat{\alpha}_{j+1/2,k}, \hat{\alpha}_{j-1/2,k}\} \hat{R}_{j,k}, \tag{4.10}$$

and the numerical flux derivatives can be calculated as

$$f'_j = \hat{A}_{j+1/2} v'_j. \tag{4.11}$$

Once again we can use the JFF and avoid the multiplication of Roe's matrix by the vector of numerical derivatives, if instead of (4.11) we employ, consult (4.9),

$$f'_{j,k} = \sum_k \text{MM}\{\hat{\alpha}_{j+1/2,k} \hat{a}_{j+1/2,k}, \hat{\alpha}_{j-1/2,k} \hat{a}_{j-1/2,k}\} \hat{R}_{j,k}. \tag{4.12}$$

As an example, let us consider the Euler equations,

$$\frac{\partial}{\partial t}\begin{bmatrix} \rho \\ m \\ E \end{bmatrix} + \frac{\partial}{\partial x}\begin{bmatrix} m \\ \rho u^2 \\ u(E+p) \end{bmatrix} = 0, \qquad p = (\gamma - 1)\cdot\left(E - \frac{1}{2}\rho u^2\right). \tag{4.13}$$

Here $\rho, u, m = \rho u, p$ and E are respectively the density, velocity, momentum, pressure, and total energy. The corresponding Roe matrix, $\hat{A}(v_j, v_{j+1})$, is associated with the eigensystem $\{\hat{a}_{j+1/2,k}, \hat{R}_{j+1/2,k}\}$, where the eigenvalues $\hat{a}_{j+1/2,k}$ are given by

$$\hat{a}_{j+1/2,1} = \hat{u}_{j+1/2} - \hat{c}_{j+1/2}, \qquad \hat{a}_{j+1/2,2} = \hat{u}_{j+1/2}, \qquad \hat{a}_{j+1/2,3} = \hat{u}_{j+1/2} + \hat{c}_{j+1/2}, \tag{4.14}$$

and the right eigenvectors are given by

$$\hat{R}_{j+1/2,1} = \begin{bmatrix} 1 \\ \hat{u} - \hat{c} \\ \hat{H} - \hat{u}\hat{c} \end{bmatrix}_{j+1/2}, \qquad R_{j+1/2,2} = \begin{bmatrix} 1 \\ \hat{u} \\ \frac{1}{2}\hat{u}^2 \end{bmatrix}_{j+1/2}, \qquad \hat{R}_{j+1/2,3} = \begin{bmatrix} 1 \\ \hat{u} + \hat{c} \\ \hat{H} + \hat{u}\hat{c} \end{bmatrix}_{j+1/2}. \tag{4.15}$$

The average quantities on the right of (4.14)–(4.15) given in [19] are

$$\hat{u} = \frac{\langle \sqrt{\rho}\, u \rangle}{\langle \sqrt{\rho} \rangle}, \qquad \hat{H} = \frac{\langle \sqrt{\rho}\, H \rangle}{\langle \sqrt{\rho} \rangle},$$

$$\hat{c} = \sqrt{(\gamma - 1)(\hat{H} - (1/2)\hat{u}^2)}, \qquad H_j = \frac{E_j + p_j}{\rho_j}, \tag{4.16}$$

where $\langle w \rangle = \frac{1}{2}(w_j + w_{j+1})$ denotes the usual arithmetic mean. This brings us to the characteristic decomposition (4.8), where the characteristic projections,

$$\hat{\alpha}_{j+1/2,1} = \frac{1}{2}(\eta_1 - \eta_2), \qquad \hat{\alpha}_{j+1/2,2} = \Delta\rho_{j+1/2} - \eta_1, \qquad \hat{\alpha}_{j+1/2,3} = \frac{1}{2}(\eta_1 + \eta_2), \tag{4.17a}$$

are expressed in terms of η_1, η_2, which are given by [19], [7]

$$\eta_1 = \Delta\rho_{j+1/2}/\hat{c}^2_{j+1/2} \tag{4.17b}$$

$$\eta_2 = (\Delta m_{j+1/2} - \Delta\rho_{j+1/2}\hat{u}_{j+1/2})/\hat{c}_{j+1/2}. \tag{4.17c}$$

We note that the second contact field associated with $\hat{R}_{j+1/2,2}$ is independent of

enforcement typical to the other two genuinely non-linear field, and therefore, is usually smeared by numerical schemes. In our next choice of numerical derivatives, we incorporate only partial characteristic information. Namely, we isolate the less expensive (i.e., square root-free) characteristic projection on the contact field and use the component-wise approach for the other two fields.

Thus, we first separate the contact field,

$$
\begin{bmatrix} \Delta\tilde{\rho}_{j+1/2} \\ \Delta\tilde{m}_{j+1/2} \\ \Delta\tilde{E}_{j+1/2} \end{bmatrix} \equiv \begin{bmatrix} \Delta\rho_{j+1/2} \\ \Delta m_{j+1/2} \\ \Delta E_{j+1/2} \end{bmatrix} - \hat{\alpha}_{j+1/2,2} \cdot \begin{bmatrix} 1 \\ \hat{u} \\ \frac{1}{2}\hat{u}^2 \end{bmatrix}_{j+1/2} , \qquad (4.18)
$$

and then define the vector of numerical derivative as

$$
\begin{bmatrix} \rho'_j \\ m'_j \\ E'_j \end{bmatrix} = \mathrm{MM}\{\hat{\alpha}_{j+1/2,2}, \hat{\alpha}_{j-1/2,2}\} \cdot \begin{bmatrix} 1 \\ \langle\hat{u}\rangle \\ \langle\frac{1}{2}\hat{u}^2\rangle \end{bmatrix}_j - \mathrm{MM}\begin{bmatrix} \Delta\tilde{\rho}_{j+1/2}, \Delta\tilde{\rho}_{j-1/2} \\ \Delta\tilde{m}_{j+1/2}, \Delta\tilde{m}_{j-1/2} \\ \Delta\tilde{E}_{j+1/2}, \Delta\tilde{E}_{j-1/2} \end{bmatrix}. \quad (4.19)
$$

Similarly, computing the numerical flux derivative with a characteristic approach applied only to the isolated contact wave,

$$
\begin{bmatrix} \Delta\tilde{f}_{j+1/2,1} \\ \Delta\tilde{f}_{j+1/2,2} \\ \Delta\tilde{f}_{j+1/2,3} \end{bmatrix} \equiv \begin{bmatrix} \Delta f_{j+1/2,1} \\ \Delta f_{j+1/2,2} \\ \Delta f_{j+1/2,3} \end{bmatrix} - \hat{\alpha}_{j+1/2,2} \cdot \hat{a}_{j+1/2,2} \cdot \begin{bmatrix} 1 \\ \hat{u} \\ \frac{1}{2}\hat{u}^2 \end{bmatrix}_{j+1/2} , \qquad (4.20)
$$

amounts to

$$
\begin{bmatrix} f'_{j,1} \\ f'_{j,2} \\ f'_{j,3} \end{bmatrix} = \mathrm{MM}(\hat{\alpha}_{j+1/2,2}\,\hat{a}_{j+1/2,2}, \hat{\alpha}_{j-1/2,2}\,\hat{a}_{j-1/2,2}) \cdot \begin{bmatrix} 1 \\ \langle u\rangle \\ \langle\frac{1}{2}\hat{u}^2\rangle \end{bmatrix}
$$
$$
- \mathrm{MM}\begin{bmatrix} \Delta\tilde{f}_{j+1/2,1}, \Delta\tilde{f}_{j-1/2,1} \\ \Delta\tilde{f}_{j+1/2,2}, \Delta\tilde{f}_{j-1/2,2} \\ \Delta\tilde{f}_{j+1/2,3}, \Delta\tilde{f}_{j-1/2,3} \end{bmatrix}. \qquad (4.21)
$$

The latter approach enables us to use effectively the artificial compression method (ACM) on the isolated contact field, e.g., [6, 7]. To this end, the contact wave isolated in (4.19) is modified by

$$
\begin{bmatrix} \rho'_j \\ m'_j \\ E'_j \end{bmatrix} = [\mathrm{MM}\{\hat{\alpha}_{j+1/2,2}, \hat{\alpha}_{j-1/2,2}\} + \theta_j r_j] \cdot \begin{bmatrix} 1 \\ \langle\hat{u}\rangle \\ \langle\frac{1}{2}\hat{u}^2\rangle \end{bmatrix}_j
$$
$$
- \mathrm{MM}\begin{bmatrix} \Delta\tilde{\rho}_{j+1/2}, \Delta\tilde{\rho}_{j-1/2} \\ \Delta\tilde{m}_{j+1/2}, \Delta\tilde{m}_{j-1/2} \\ \Delta\tilde{E}_{j+1/2}, \Delta\tilde{E}_{j-1/2} \end{bmatrix}_j , \qquad (4.22a)
$$

where θ_j and r_j are given by

$$
\theta_j = \frac{|\hat{\alpha}_{j+1/2,2} - \hat{\alpha}_{j-1/2,2}|}{|\hat{\alpha}_{j+1/2,2}| + |\hat{\alpha}_{j-1/2,2}|}, \qquad (4.22b)
$$

$$
r_j = \mathrm{MM}\{\tfrac{1}{2}(1 - \lambda\hat{u}_{j+1/2})^2 \cdot \hat{\alpha}_{j+1/2,2}, \tfrac{1}{2}(1 - \lambda\hat{u}_{j-1/2})^2 \cdot \hat{\alpha}_{j-1/2,2}\}. \qquad (4.22c)
$$

Finally, we shall mention an alternative approach to the characteristic implementation of the ACM in (4.22). To this end, the artificial compression is implemented as a further corrector step to the component-wise approach presented in (4.2a)–(4.2b). This corrective type ACM takes the form,

$$v_j^*(t + \Delta t) = v_j(t + \Delta t) - \varepsilon(W_{j+1/2} - W_{j-1/2}), \qquad 0 \leqslant \varepsilon \leqslant 1. \qquad (4.23a)$$

Here, the compression coefficient, ε, and W_j are given by

$$W_{j+1/2} = \begin{cases} w_j, & \Delta w_{j+1/2} \cdot \Delta v_{j+1/2} > 0, \\ w_{j+1}, & \Delta w_{j+1/2} \cdot \Delta v_{j+1/2} < 0, \end{cases} \qquad w_j = \mathrm{MM}\{\Delta v_{j-1/2}, v_{RL}, \Delta v_{j+1/2}\},$$

$$(4.23b)$$

where v_{RL} is related to subcell resolution information (Harten, private communication, [8]),

$$v_{RL} = |v_{j+1}(t + \Delta t) - v_{j-1}(t + \Delta t) - \Delta x_{j+1/2}(\delta_{j+1} + \delta_{j-1})|,$$
$$\delta_j = \mathrm{MM}\{\Delta v_{j-1/2}, \Delta v_{j+1/2}\}. \qquad (4.23c)$$

The result is the central differencing scheme (4.2), appended by the component-wise definitions of numerical derivatives in (4.4)–(4.6), and complemented by the ACM corrector step (4.23). This scheme, unlike the characteristic-wise implementation of the ACM in (4.22), enjoys the simplicity of the component-wise approach, and at the same time, enables us to deal effectively with the delicate contact wave. We remark that one should be careful not to overcompress discontinuities using such corrective type artificial compression: it should be implemented after the rarefaction waves have evolved using an appropriately chosen compression coefficient ε.

5. NUMERICAL EXAMPLES

In this section, we will present numerical examples which demonstrate the performance of our family of high resolution central differencing schemes for systems of conservation laws. We consider the approximate solution of the Euler equations of gasdynamics, see Section 4,

$$\frac{\partial}{\partial t} \begin{bmatrix} \rho \\ m \\ E \end{bmatrix} + \frac{\partial}{\partial x} \begin{bmatrix} m \\ \rho u^2 \\ u(E + p) \end{bmatrix} = 0, \qquad p = (\gamma - 1) \cdot \left(E - \frac{1}{2}\rho u^2\right), \; m = \rho u. \qquad (5.1)$$

We experiment with the following members from our family of high-resolution central differencing schemes:

1.   The central differencing scheme (4.2), (4.4a), (4.5). This is the component-wise extension of the scalar STG scheme presented in Section 3 and is therefore referred to by the same abbreviation.

2.   The central differencing scheme (4.2), (4.4b), (4.5) with a limiter value $\alpha = 2$. This scheme is referred to as STG2.

3.   The component-wise UNO-type version of our scheme, (4.2), (4.4c), (4.5). It is referred to as STGU.

4.   The scheme STG with the addition of the corrective type ACM described by (4.23) is referred to as STGC.

All the above examples use component-wise definitions for the vectors of numerical derivatives, and are based on the staggered grid formulation. Our last example is based on non-staggered LxF scheme, namely,

5.   The central differencing scheme (2.18), (4.4a), (4.5). This is the component-wise extension of the scalar ORD scheme presented in Section 3 and is therefore reffered to by the same abbreviation.

For the purpose of performance comparison we include here the results of several well-known upwind and central schemes as well. These schemes include:

1.   The first-order central non-staggered LxF scheme, (2.17) [13].

2.   The first-order accurate Godunov-type scheme of Roe, e.g. [7].

3.   Harten's second-order accurate upwind ULT1 scheme, [7].

4.   Harten's second-order accurate upwind ULT1C scheme, [7], where artificial compression is added to ULT1 in the linearly degenerate contact field. It is referred to as ULTC.

We solve the system (5.1) with three sets of initial conditions. Our first example is the Riemann problem proposed by Sod [21] (abbreviated hereafter as RIM1), which consists of initial data

$$v(x, 0) = \begin{cases} v_l, & x < 0,\ v_l = (1, 0, 2.5)^{\mathrm{T}} \\ v_r, & x > 0,\ v_r = (0.125, 0, 0.25)^{\mathrm{T}}. \end{cases} \tag{5.2}$$

Table II shows the time performance of the various schemes. All the schemes have time performances of order $O(NX)^2$, where NX is the number of spatial cells. Table III shows the L_1 norm of the errors. Though the results are field dependent, the "quatitative picture" is favourable with the central differencing schemes. Figures 5.1–5.3 include a comparison between the numerical solution and the exact solution (shown by the solid line), e.g., [3, 20], at $t = 0.1644$. As expected, the overall resolution of the first order schemes is outperformed by the second order schemes.

We observe that our second-order staggered schemes, STG, STG2, and STGU, and similarily, the second-order upwind ULT1 scheme, smear the shock discontinuity over two cells. The contact discontinuity, however, is more delicate: here we

TABLE II

Computation Time of Riemann Problems, Results at $t = 1.0$

	ULT1/C	STG	ROE	ORD	LxF	STGC	STGU	STG2	NX
RIM1									
	1.23	1.23	0.74	0.69	0.22	1.43	1.47	1.37	50
	4.93	4.75	2.92	2.71	0.85	5.67	5.88	5.43	100
	19.81	19.32	11.68	10.71	3.37	22.74	23.49	21.66	200
RIM2									
	2.87	2.74	1.72	1.55	0.48	3.24	3.35	3.07	50
	11.54	10.93	6.83	6.16	1.90	12.88	13.30	12.22	100
	46.34	43.50	27.27	24.40	7.52	51.46	53.20	48.83	200

Notes. 1. Due to our method of implementation, ULT1 and ULTC have the same computation time. In fact, ULT1 is somewhat faster then ULTC.

2. All the above schemes use a CFL number of 0.95, except for the versions, STG*, which use a CFL number of 0.475.

TABLE III

Riemann Problems, L_1 Norm Errors

	Density			Velocity			Pressure		
Nx	50	100	200	50	100	200	50	100	200
Scheme									

Riemann Problem—RIM1, $t = 0.1644$

	50	100	200	50	100	200	50	100	200
LxF	0.03121	0.02460	0.01769	0.06651	0.04583	0.02814	0.03602	0.02458	0.01582
ROE	0.01918	0.01308	0.00836	0.03224	0.02090	0.01145	0.01762	0.01109	0.00666
ORD	0.01868	0.01026	0.00578	0.03315	0.01807	0.00959	0.01630	0.00861	0.00460
STG	0.01495	0.00741	0.00409	0.02812	0.01105	0.00550	0.01232	0.00581	0.00294
ULT1	0.01338	0.00806	0.00437	0.02933	0.01177	0.00820	0.01285	0.00736	0.00362
STG2	0.1241	0.00619	0.00297	0.02449	0.01132	0.00494	0.01019	0.00487	0.00228
STGU	0.01146	0.00544	0.00291	0.02300	0.00816	0.00403	0.00961	0.00432	0.00216
STGC	0.00982	0.00322	0.00172	0.01994	0.00481	0.00276	0.00705	0.00270	0.00153
ULTC	0.01269	0.00715	0.00361	0.02923	0.01761	0.00804	0.01283	0.00735	0.00362

Riemann Problem—RIM2, $t = 0.16$

	50	100	200	50	100	200	50	100	200
LxF	0.12162	0.09044	0.06165	0.13523	0.09294	0.05557	0.15860	0.10767	0.06537
ROE	0.06630	0.04334	0.02827	0.07397	0.04144	0.02192	0.08399	0.04826	0.02655
ORD	0.06791	0.03824	0.02231	0.07158	0.03623	0.01709	0.07836	0.04056	0.01995
STG	0.04972	0.02903	0.01776	0.04392	0.02416	0.01307	0.05118	0.02669	0.01426
ULT1	0.04518	0.03572	0.01477	0.05570	0.02603	0.01094	0.06075	0.02841	0.01206
STG2	0.03473	0.02129	0.01151	0.03369	0.01655	0.00849	0.03956	0.02037	0.00988
STGU	0.03668	0.02152	0.01302	0.03323	0.01657	0.01046	0.03907	0.02031	0.01121
STGC	0.02764	0.01291	0.00647	0.02285	0.01356	0.00836	0.02355	0.01409	0.00873
ULTC	0.03001	0.01566	0.00872	0.05504	0.02545	0.01074	0.05997	0.02784	0.01183

Notes. 1. All the above schemes use CFL number of 0.95, except for the staggered versions, STG*, which use a CFL number of 0.475.

2. The underlined results indicate the smallest L_1 norm errors in every column.
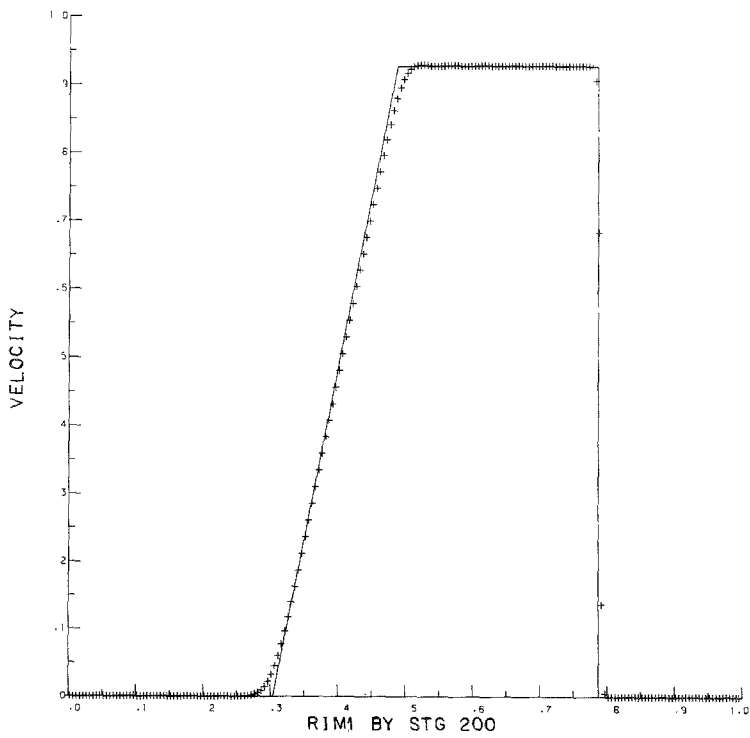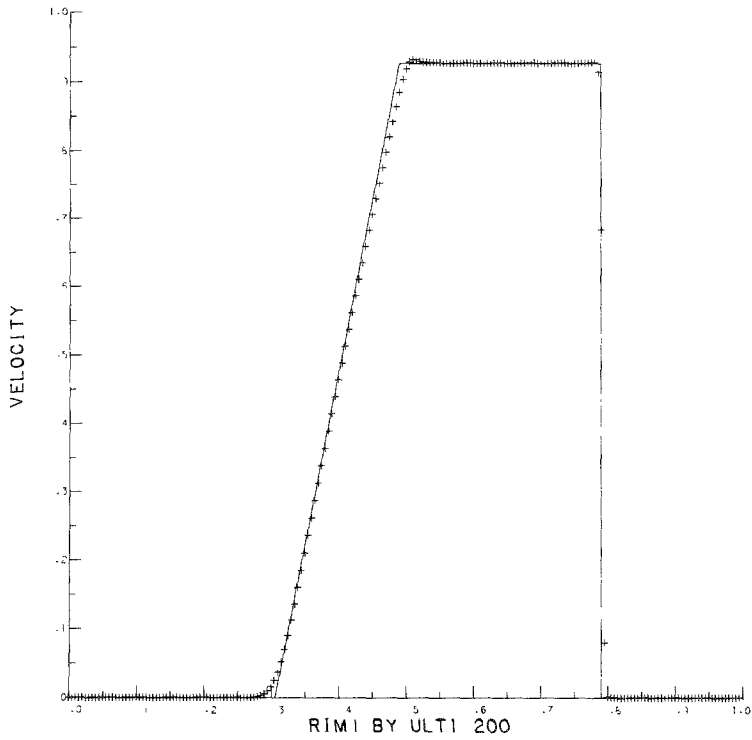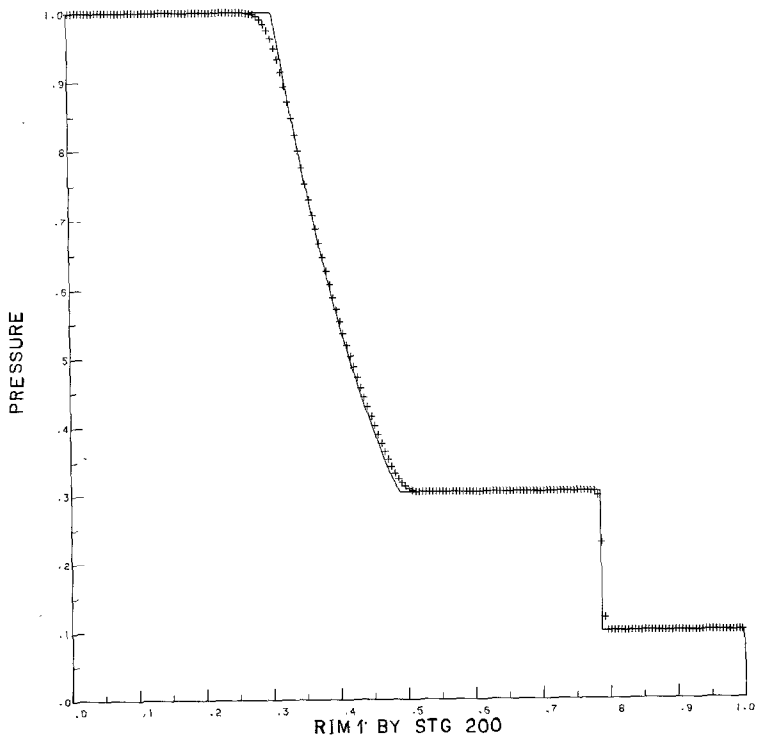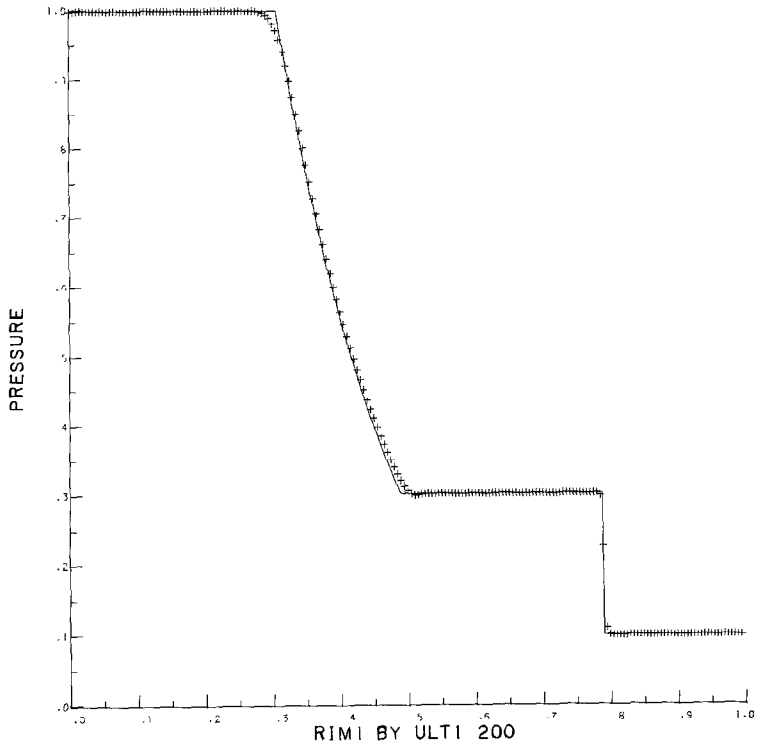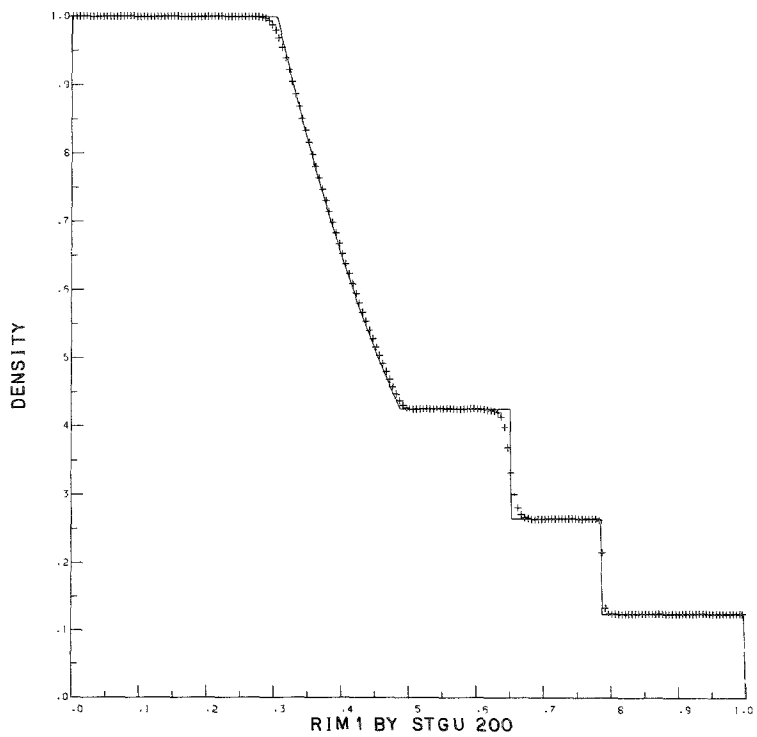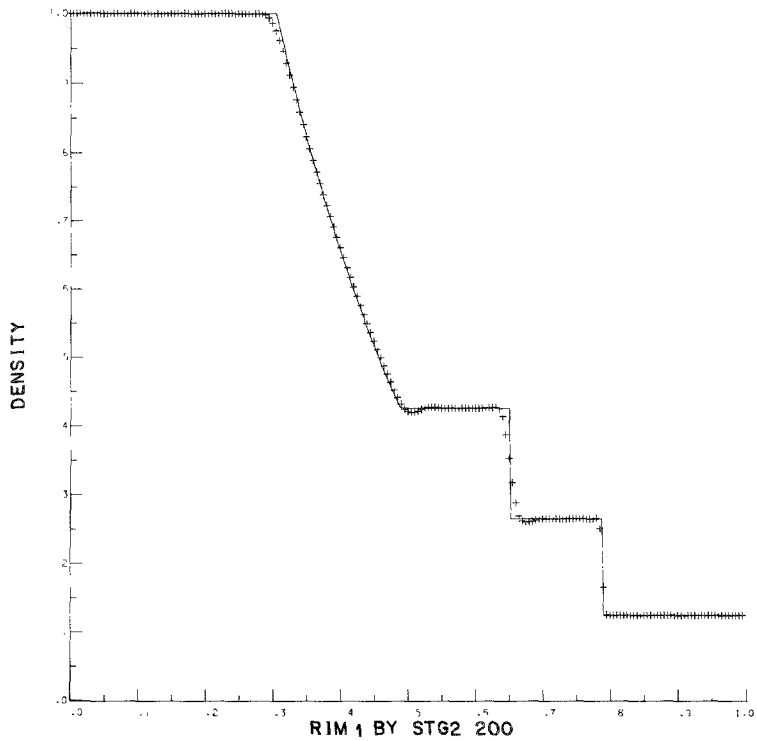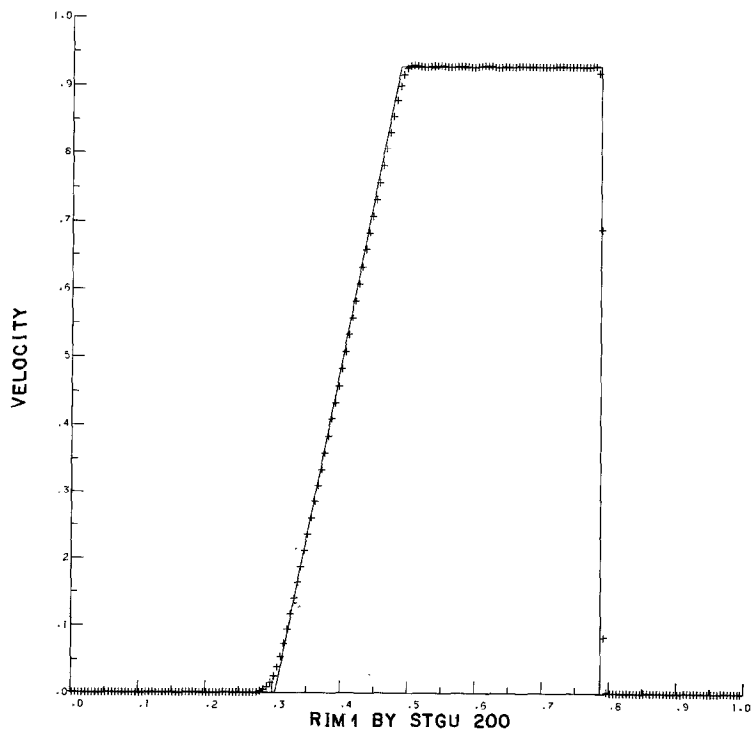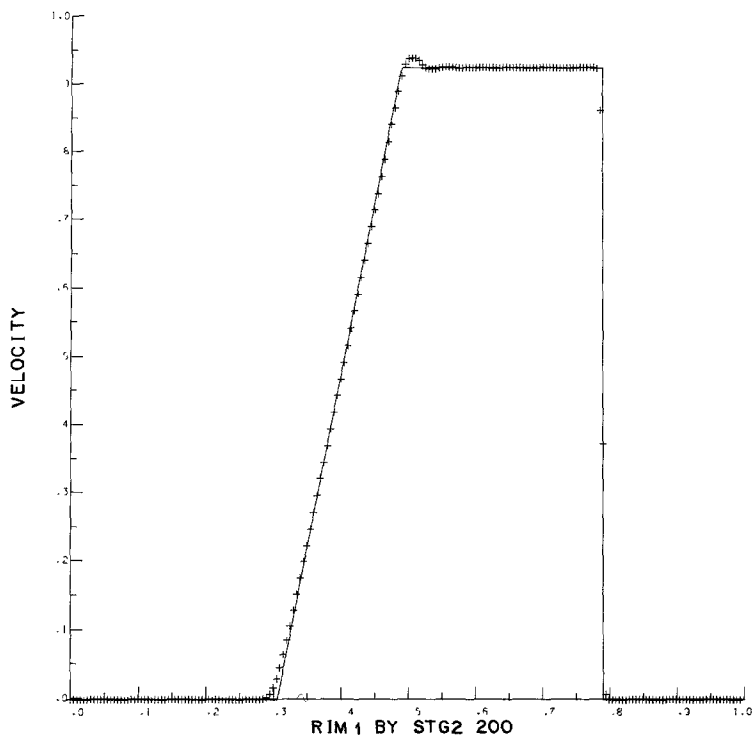
RIM1 BY ULT1 200

RIM1 BY STG 200

FIG. 5.1—*Continued*

435

FIG. 5.1—*Continued*

436

FIGURE 5.2

437

FIG. 5.2—*Continued*

438

FIG. 5.2—*Continued*
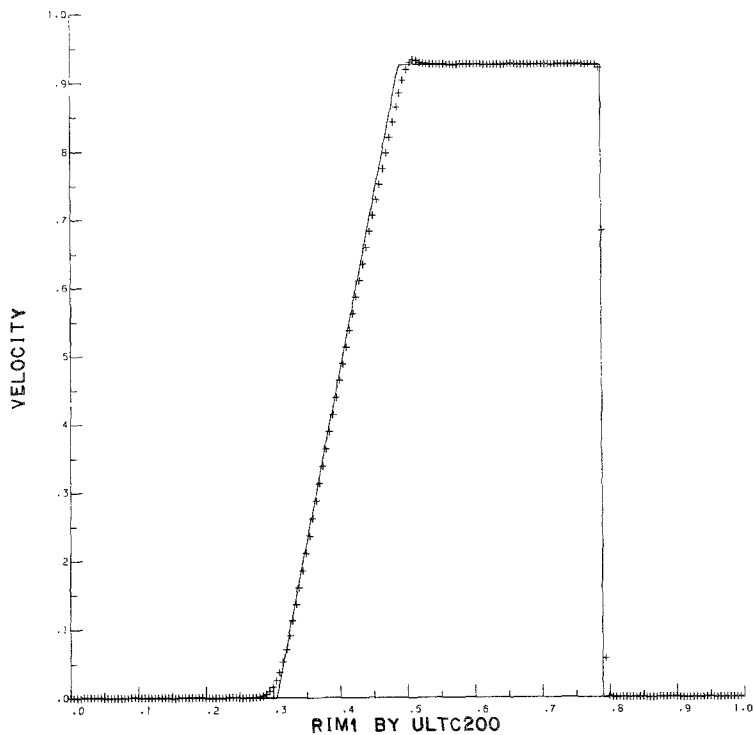
439

FIGURE 5.3

440
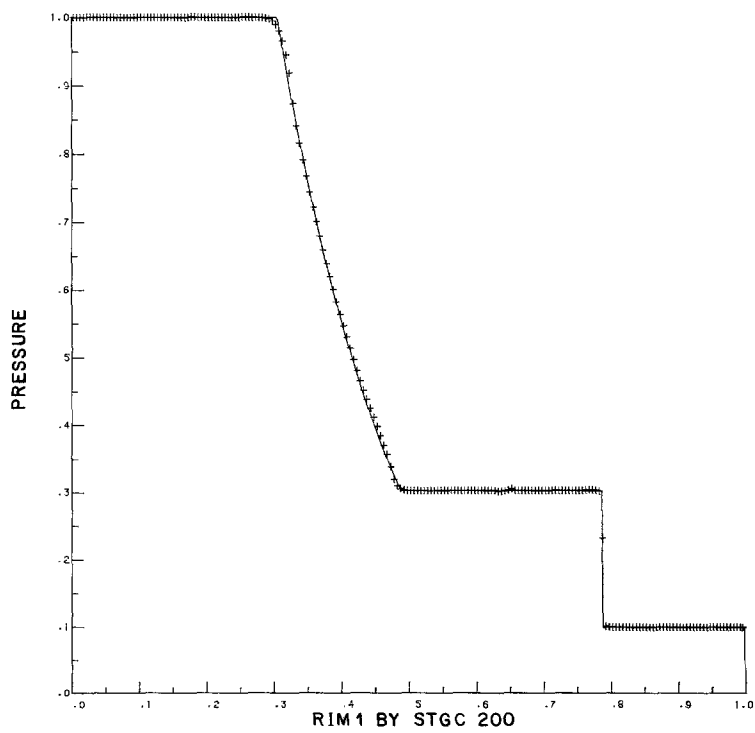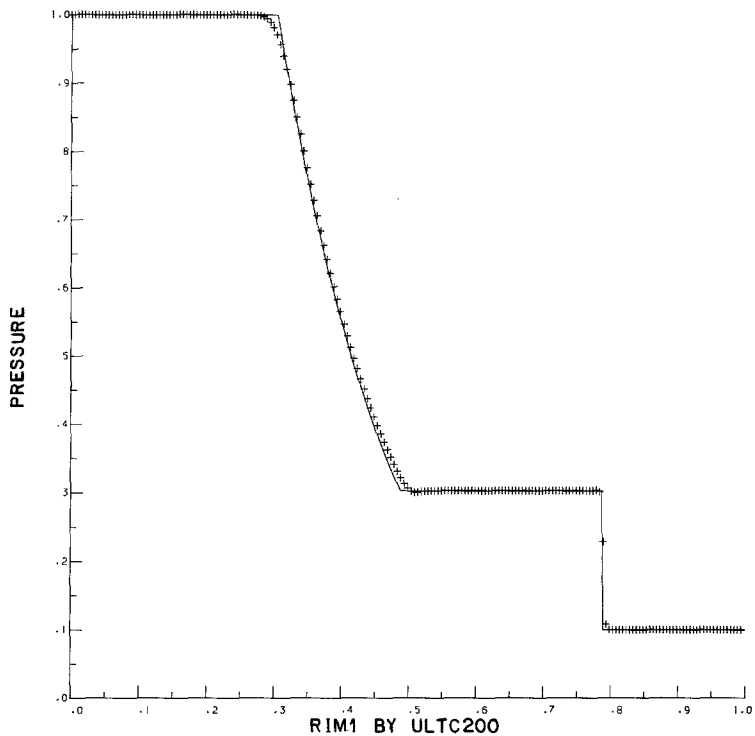
FIG. 5.3—*Continued*

441

FIG. 5.3—*Continued*

442
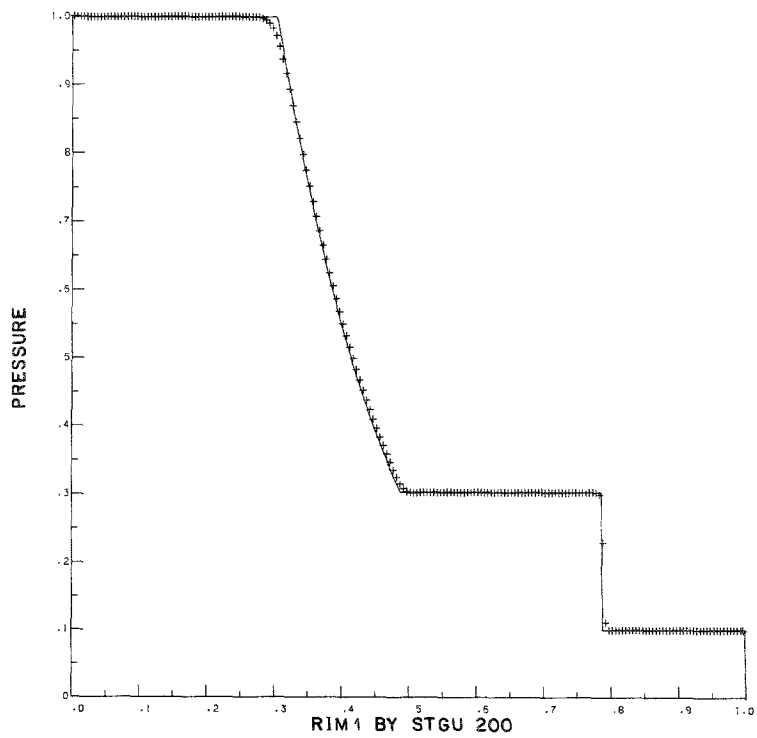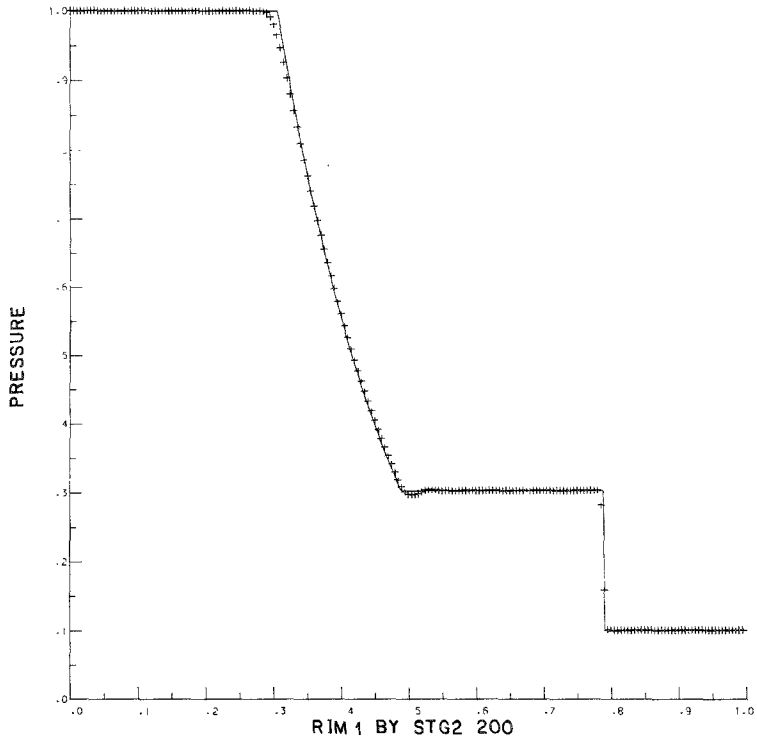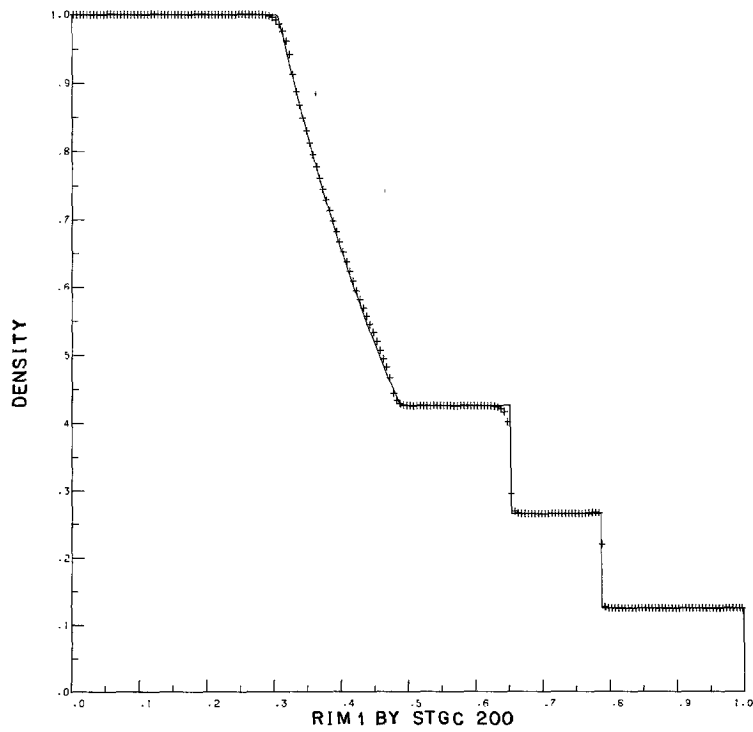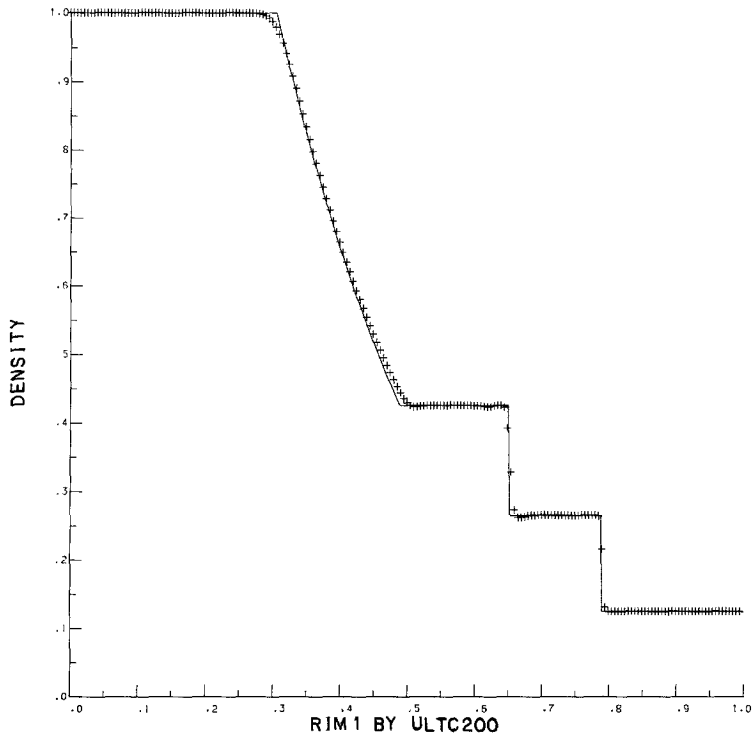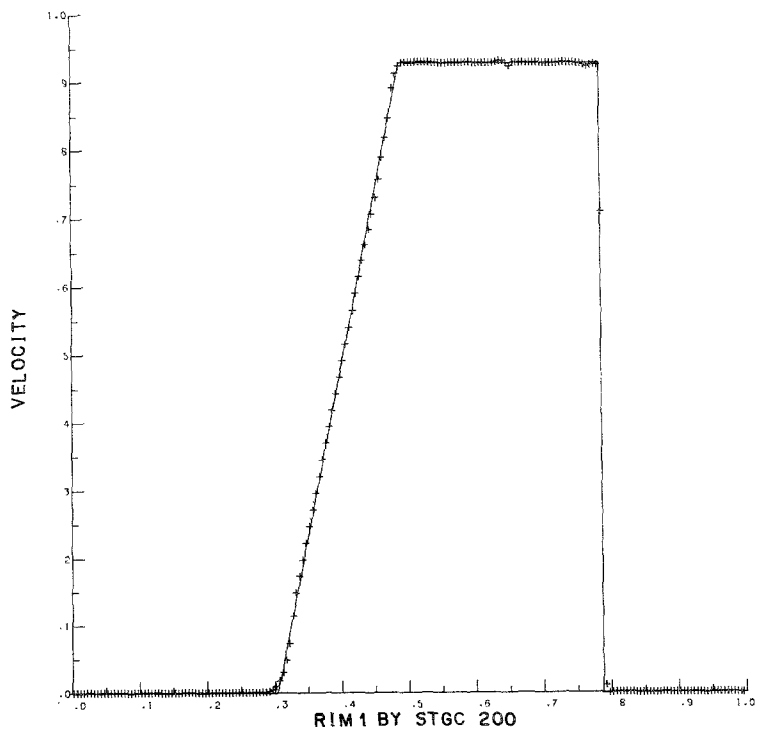
observe smearing of about 5–6 cells by the second-order schemes, both in the central and upwind cases. We can also observe the over- and undershoots generated by both the upwind ULT1 and central STG2. These unsatisfactory results suggest to introduce ACM in the contact field. For this purpose we present the upwind ULTC scheme and the central component-wise STGC scheme in Fig. 5.3. We note that the ACM is applied in STGC only at the last 10% of the time steps with the compression coefficient $\varepsilon = 0.625$. This results in two cells resolution of the contact wave and somewhat better resolution in the other waves as well. Yet, small over- and undershoots which are due to overcompression, still remain.

Our second Riemann test problem (abbreviated hereafter as RIM2) is the one proposed by Lax [13]. It is initiated with,

$$v_l = (0.445, 0.311, 8.928)^T, \qquad v_r = (0.5, 0, 1.4275)^T, \tag{5.3}$$

and the results at $t = 0.16$ can be found in Figs. 5.4–5.6. The density profile in RIM2 lacks the monotonicity we had in RIM1, and therefore, it is more difficult for "non-oscillatory" numerical schemes to recover the contact wave and the intermediate "plateau" which follows. Consequently, the upwind schemes perform here somewhat better than the central schemes: ULTC resolution is better than STGC which has more over- and undershoots than before. We note that STG2 has better resolution and L_1 errors than STGU in all fields. This is due to the fact that STG2 has steeper slope near discontinuities, consult Section 2. For comparison purposes, we also included, in Fig. 5.5, the results of the nonstaggered central difference scheme ORD for the RIM2 problem. We recall that the CFL limitation in the staggered case, $\beta \lesssim \frac{1}{2}$, is now doubled to be $\beta \lesssim 1$, consult Section 3. Moreover, a component-wise reconstruction of the vector of numerical derivatives, enabled us to avoid any Riemann solver in this nonstaggered case. Consequently, the ORD scheme is two times faster than the staggered central versions based on STG, as well as the upwind scheme ULT1 which necessitates the (approximate) solution of a Riemann problem at each cell. However, the resolution of this nonstaggered version, ORD, deteriorates when compared to the staggered versions and the upwind methods. Finally, we note that the upgrade from the first-order LxF to either STG or ORD versions, results in a substantial improvement in resolution.

Our third problem, discussed by Woodward and Collela in [25], consists of

$$u(x, 0) = \begin{cases} v_l, & 0 \leqslant x < 0.1, \\ v_m, & 0.1 \leqslant x < 0.9, \\ v_r, & 0.9 \leqslant x < 1, \end{cases} \tag{5.4}$$

where $\rho_l = \rho_m = \rho_r = 1$, $m_l = m_m = m_r = 0$, $p_l = 100$, $p_m = 0.01$, $p_r = 100$. A solid wall boundary conditions (reflection) is applied to both ends. We present the results of STG2 and ULT1 with 400 cells in Figs. 5.7–5.8 at $t = 0.03$ and $t = 0.038$ respectively. We observe that STG2 compares favourably with the second-order upwind ULT1
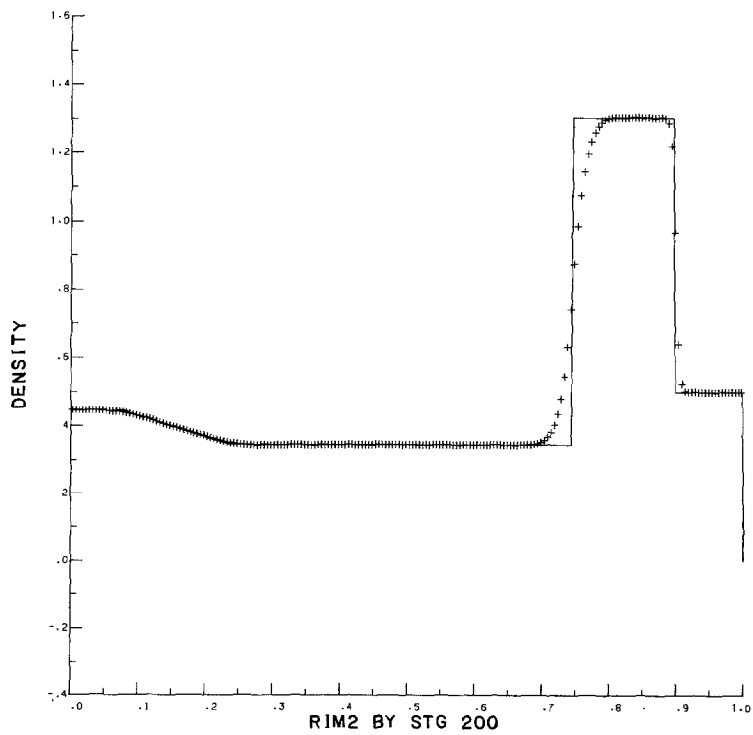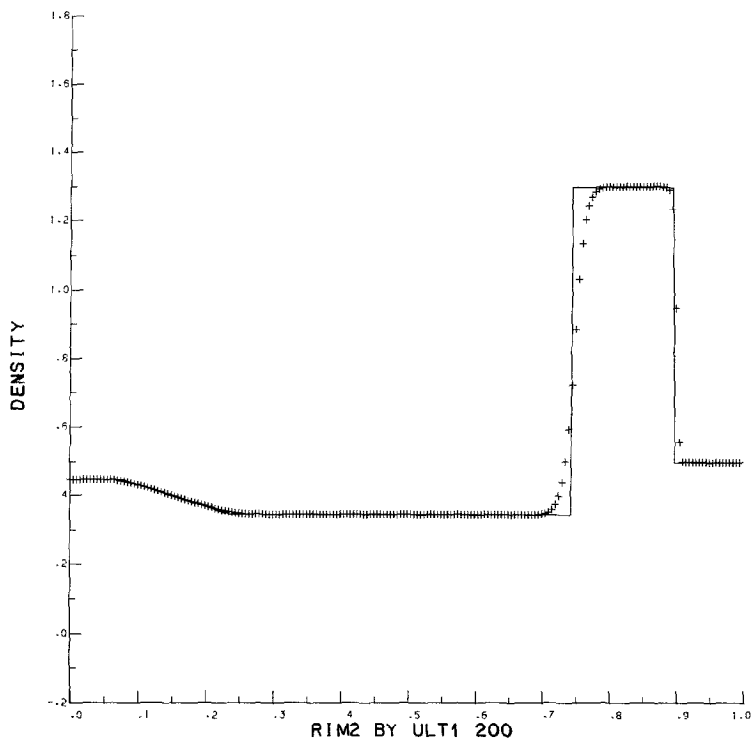
FIGURE 5.4
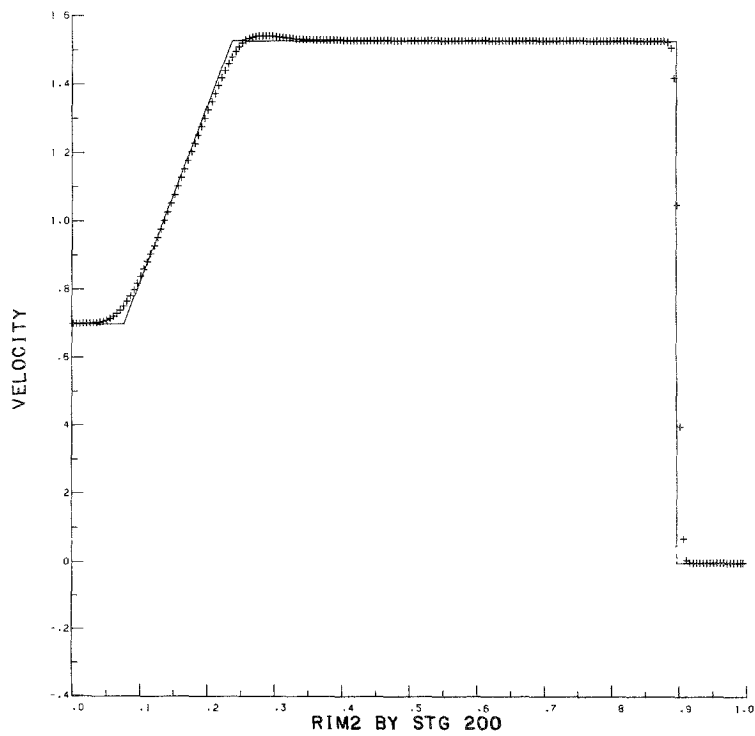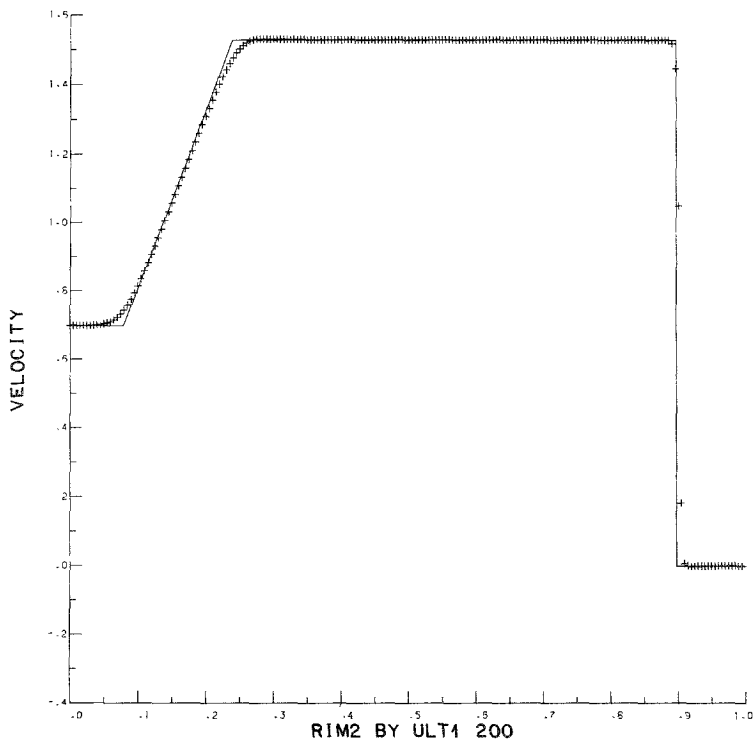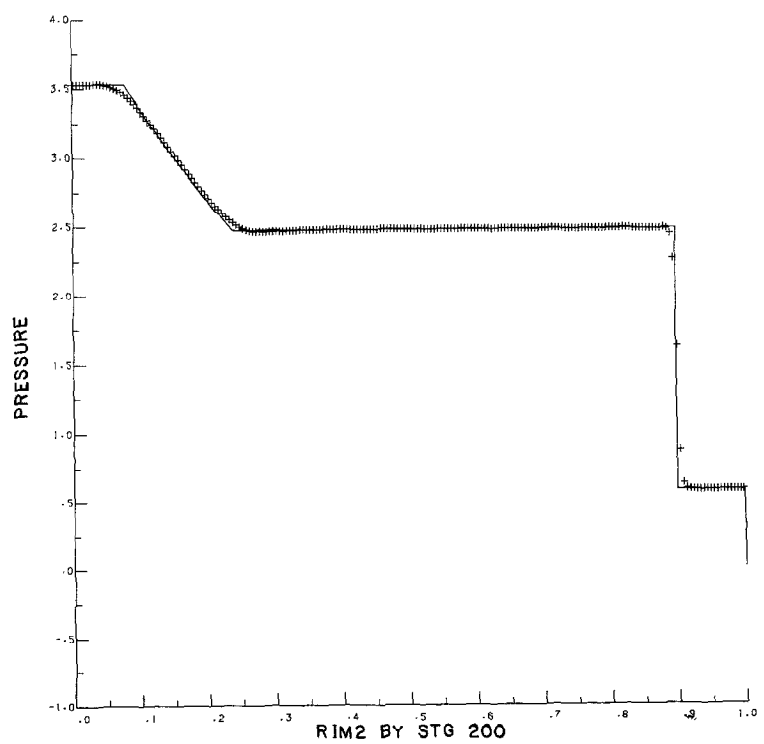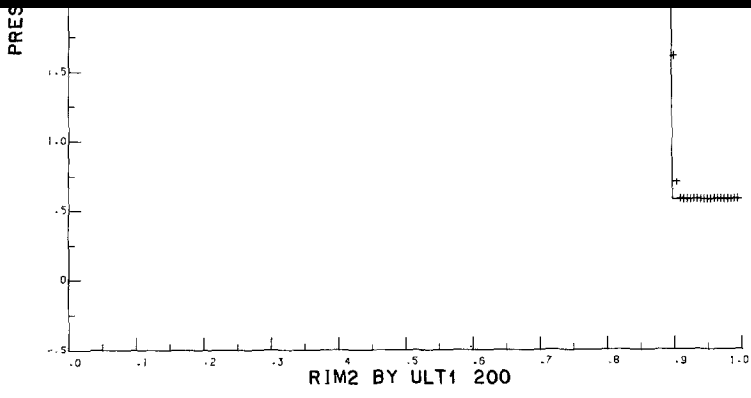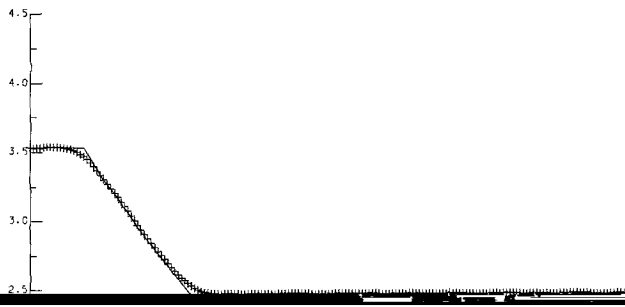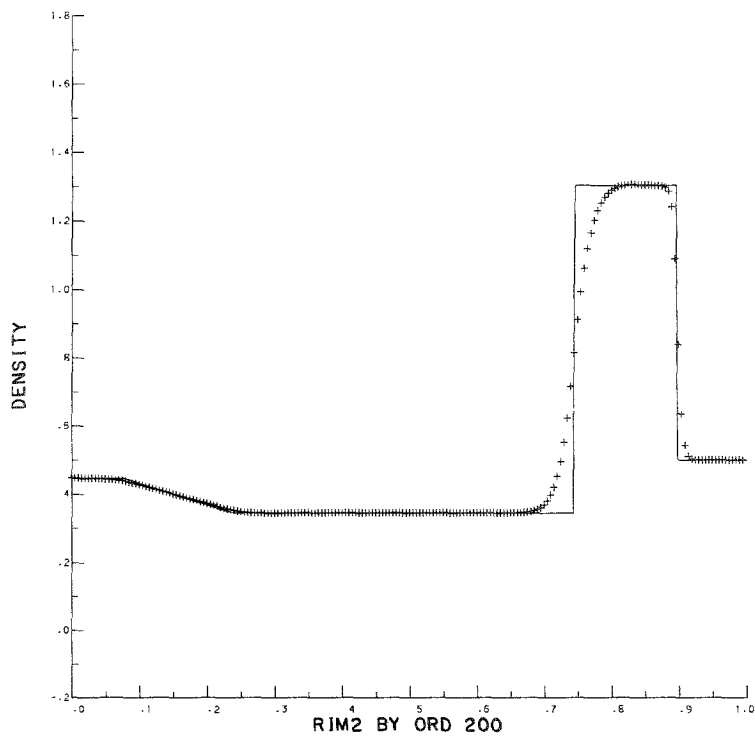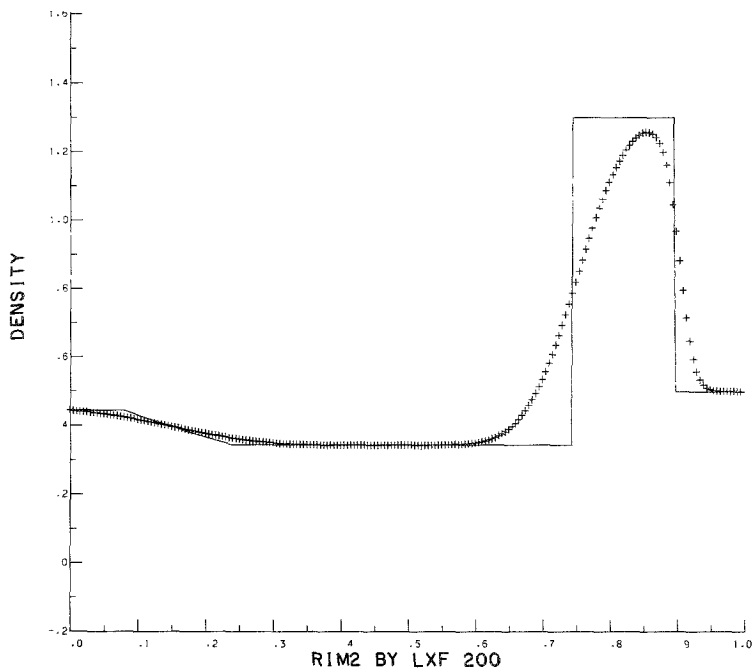
444

FIG. 5.4—*Continued*

445

FIG. 5.4—*Continued*

446

FIGURE 5.5

447

RIM2 BY LXF 200

RIM2 BY ORD 200

FIG. 5.5—*Continued*

449

FIGURE 5.6

450

RIM2 BY ULTC 200

RIM2 BY STGC 200

FIG. 5.6—*Continued*

451

FIG. 5.6—*Continued*

452

FIGURE 5.7
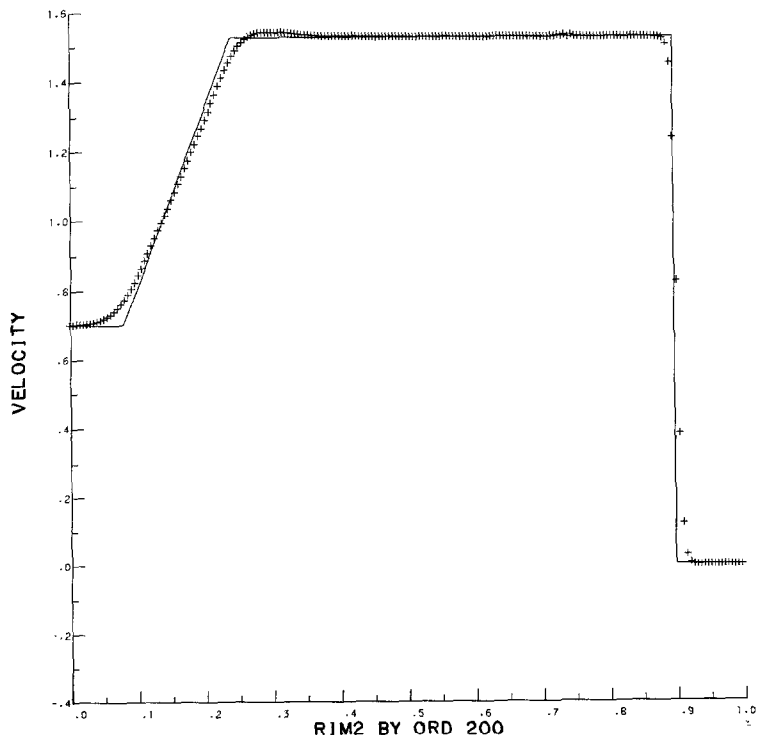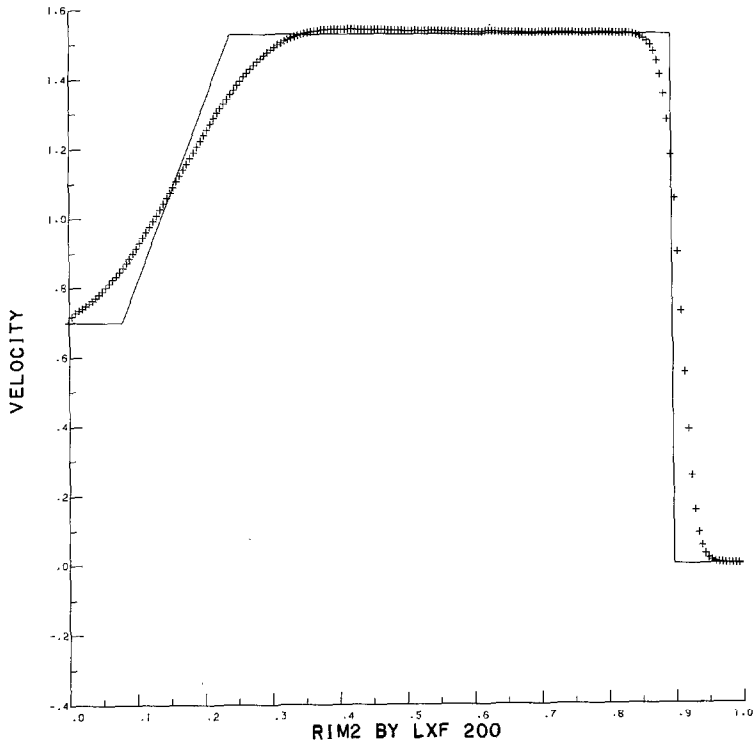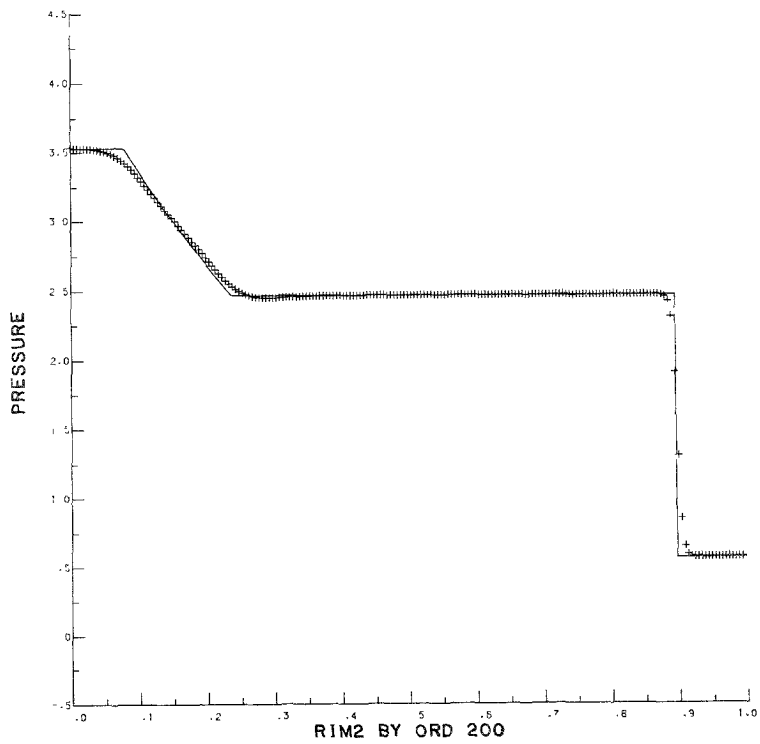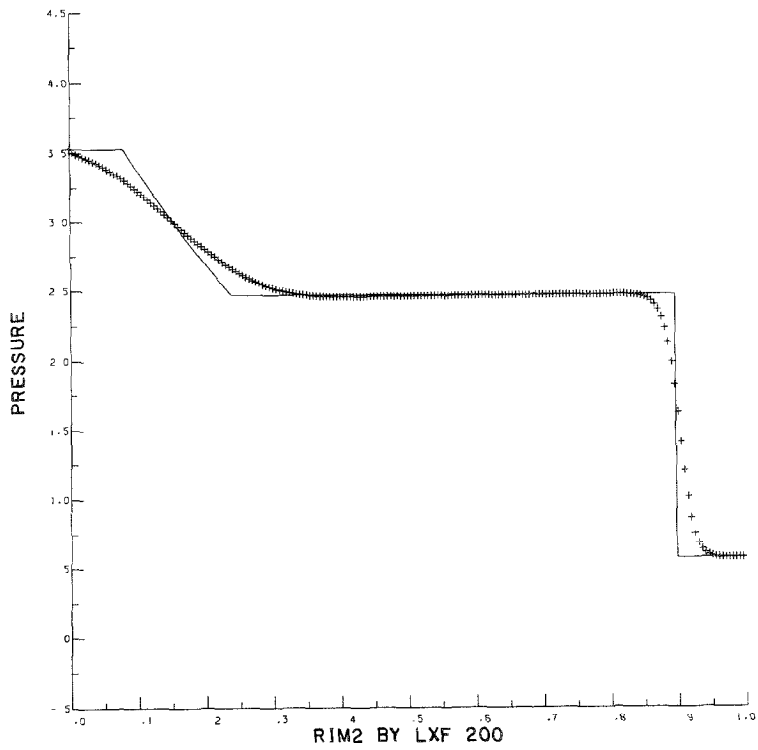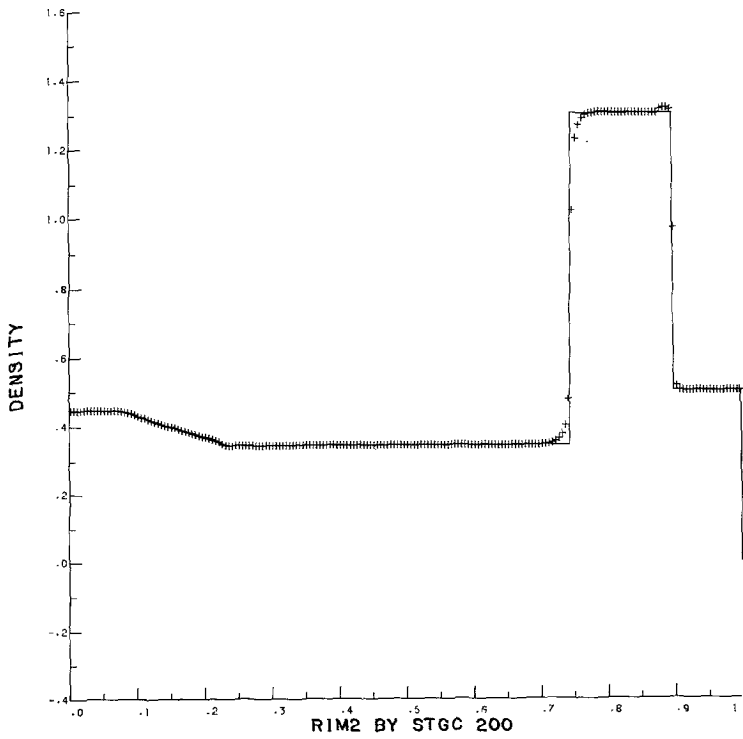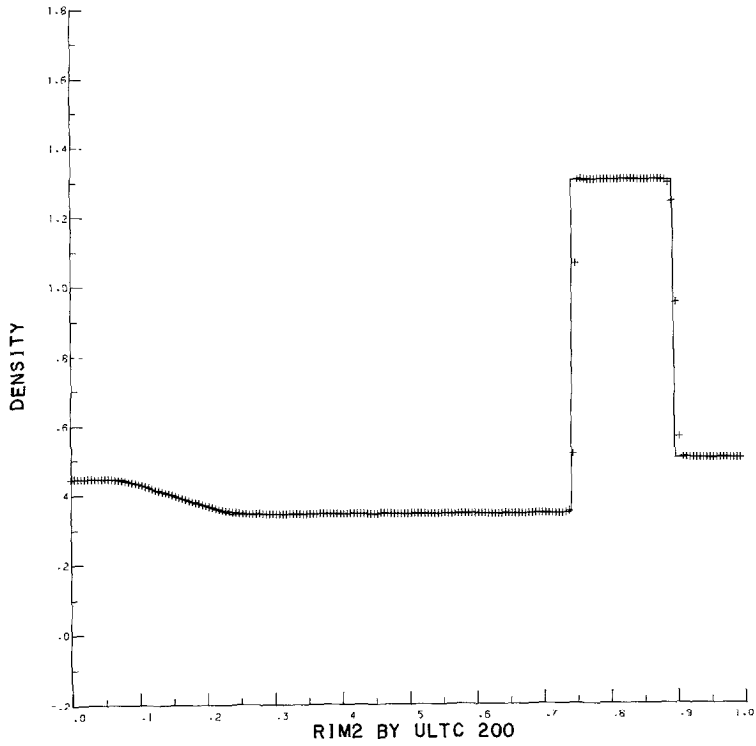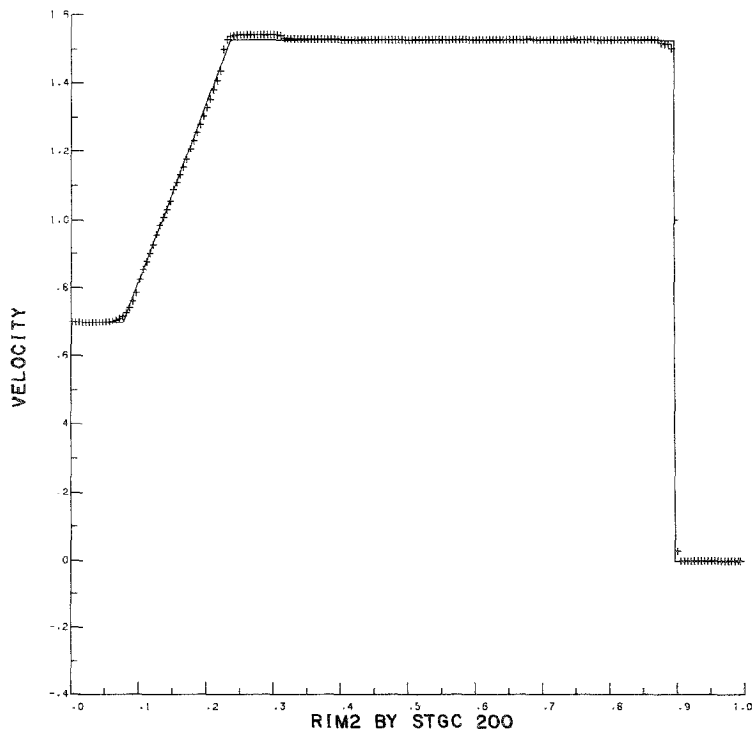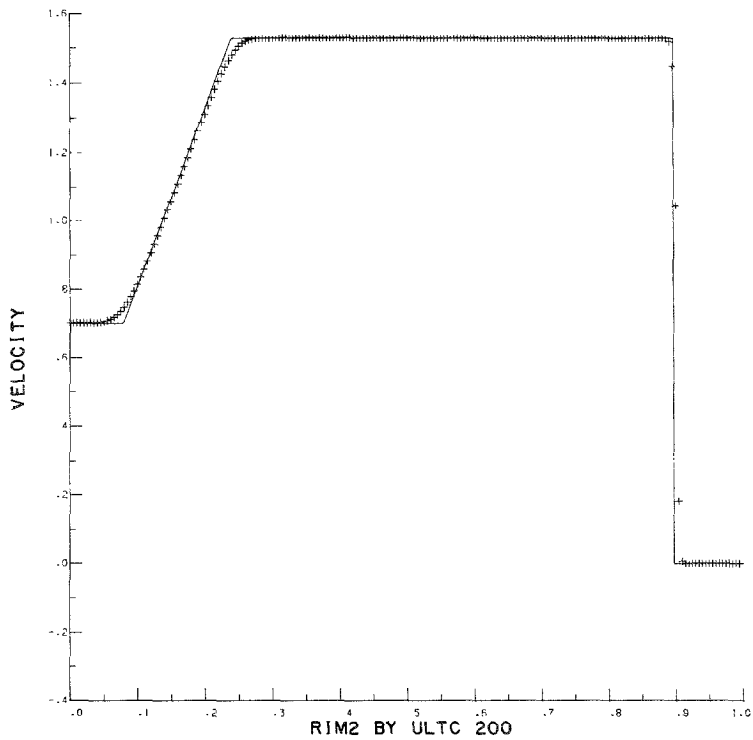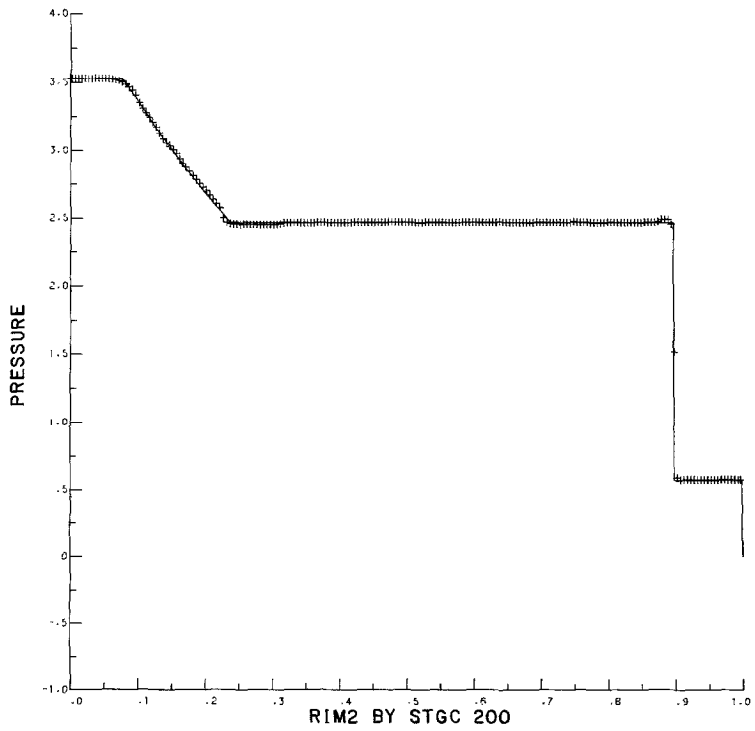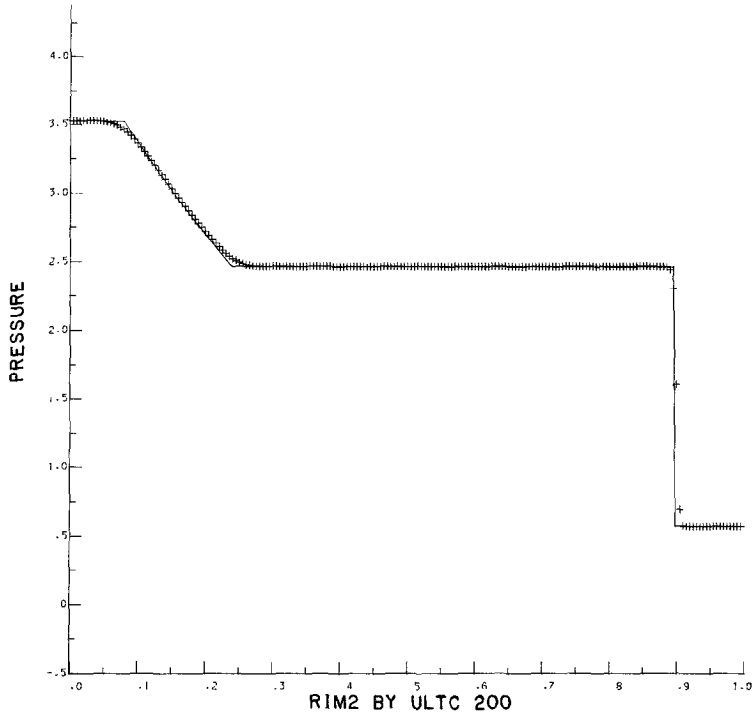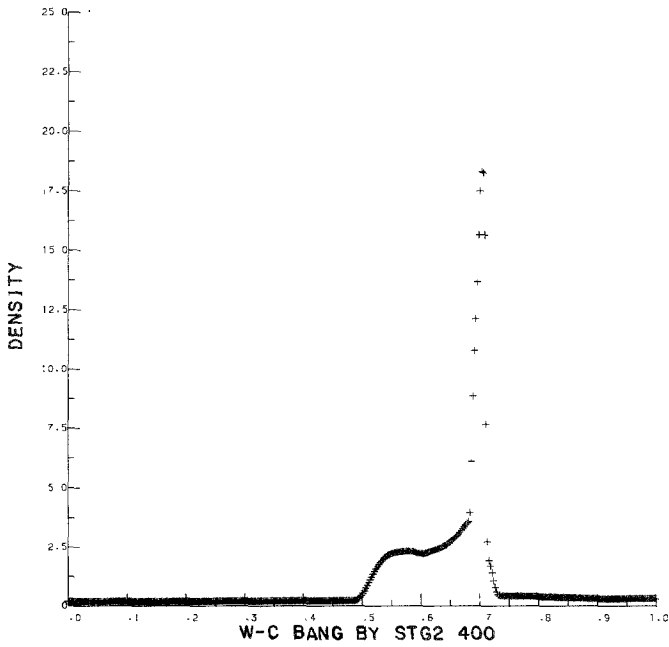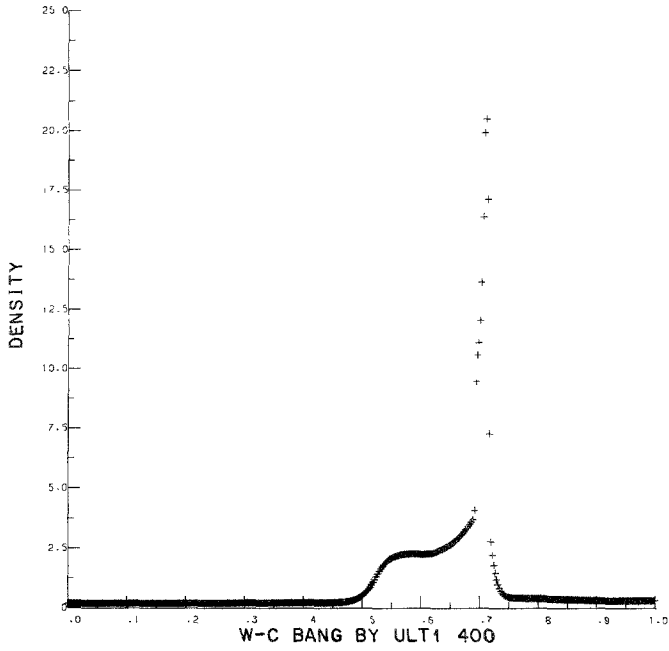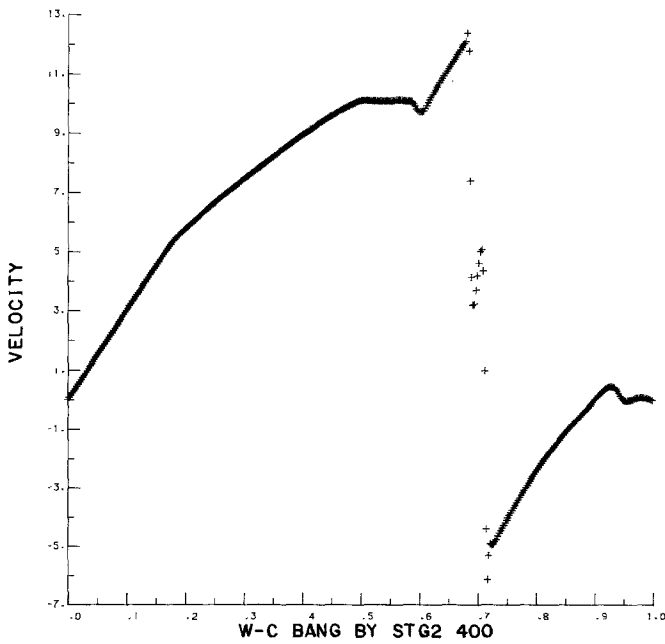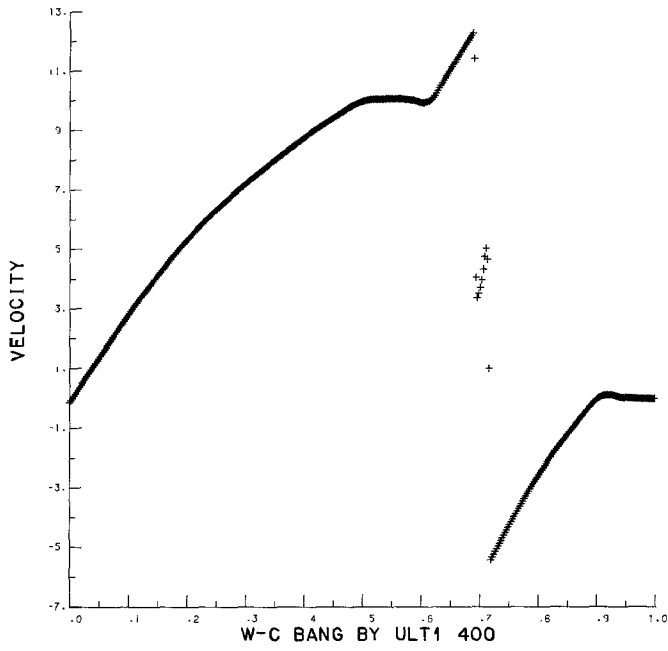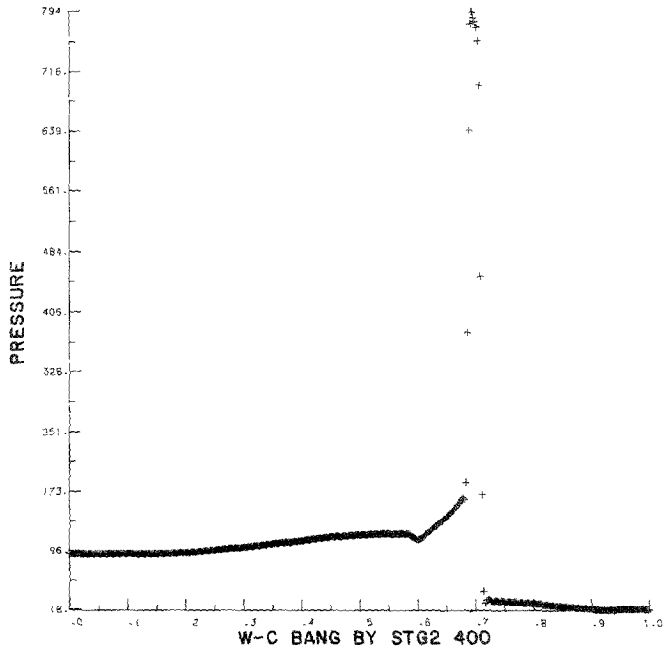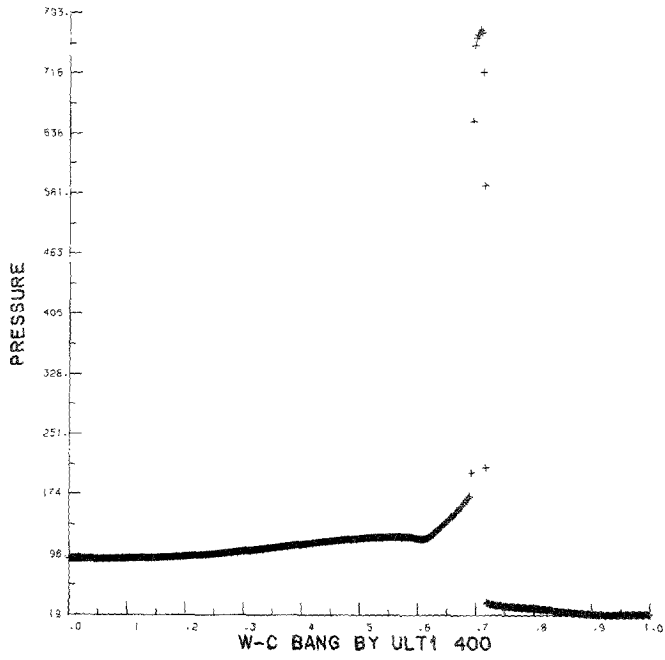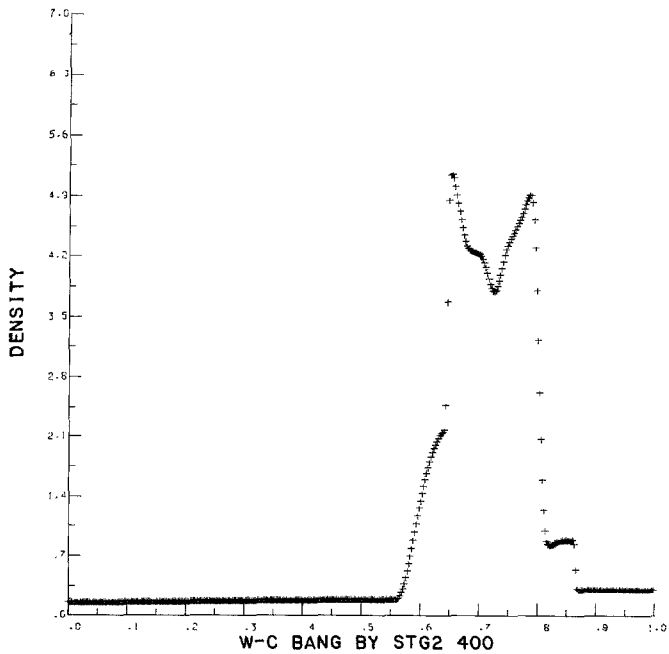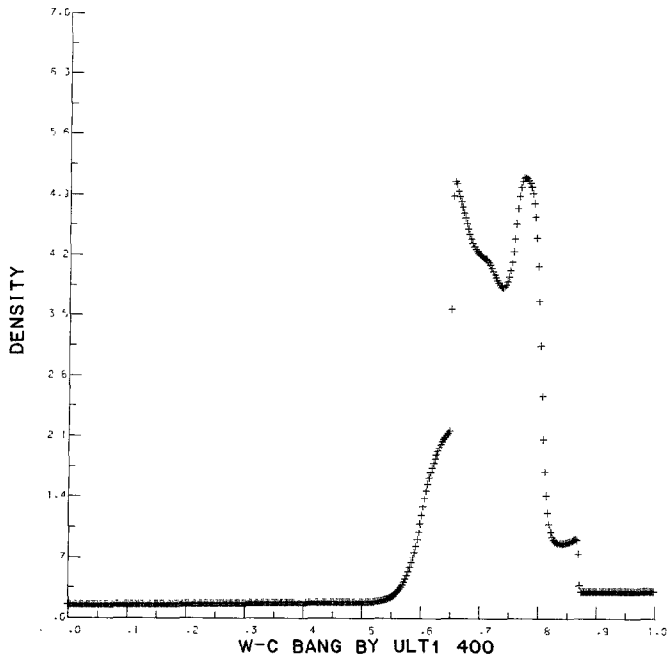
W-C BANG BY ULT1 400

W-C BANG BY STG2 400
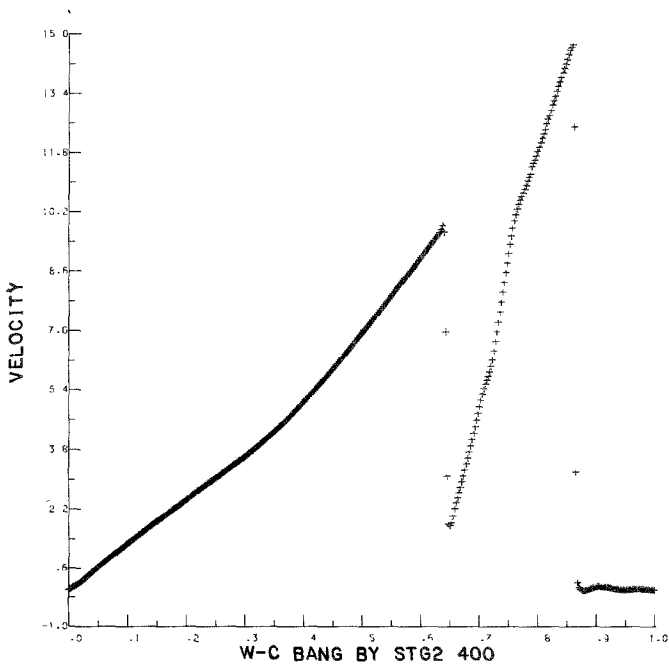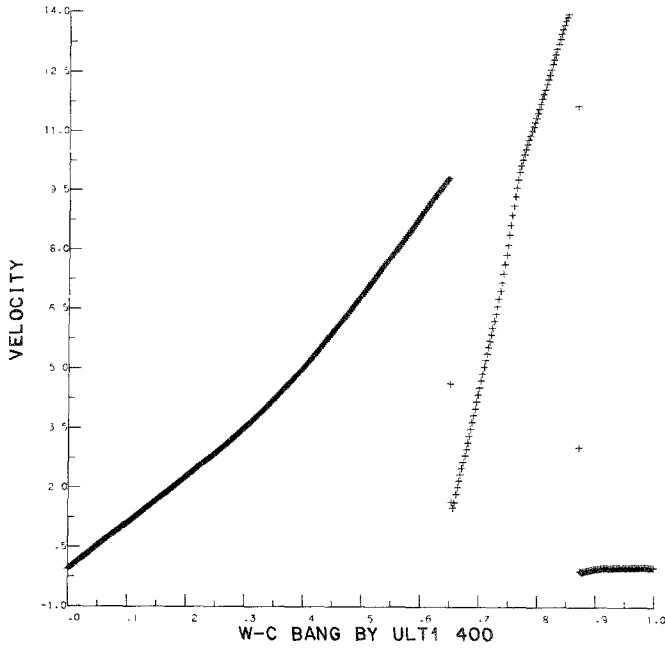
FIG. 5.7—*Continued*

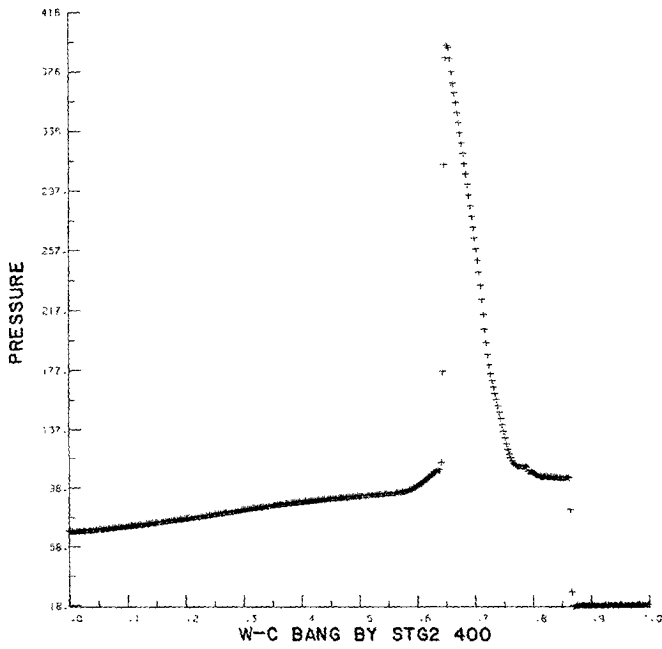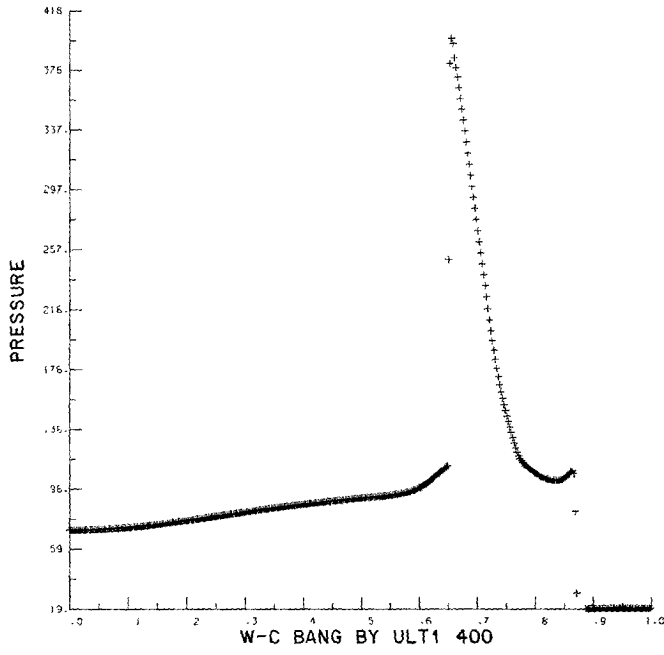FIG. 5.7—Continued

FIGURE 5.8

FIG. 5.8—*Continued*

FIG. 5.8—Continued

scheme. The evolution of the Woodward–Collela problem (5.4) is governed by a complicated series of wave interactions [25]. Therefore, the numerical results of the STG2 scheme in Figs. 5.7–5.8 are particularly instructive, since they are based on a simple component-wise reconstruction and do not involve any field-by-field decomposition.

In summary, we may conclude that when strong discontinuities are present, STG2 seems to offer the best results, STGC can be tuned to obtain sharp resolution at the expense of overcompression, and the ORD version was found to be the most economical. Further extensive numerical experiments done along these lines are reported in [16].

APPENDINX: On a Cell Entropy Inequality

In this section, we provide the promised proofs for Lemmatta 3.5 and 3.6, which verify the cell entropy inequality for our family of scalar high-resolution central difference methods.

We begin with a proof of Lemma 3.5. Let $R_{j+1/2}(g)$ denote the difference,

$$R_{j+1/2}(g) = \tfrac{1}{2}\left[U(v_{j+1}) + U(v_j)\right] - \lambda \int_{v_j}^{v_{j+1}} U'(v)\,g'(v)\,dv - U(v_{j+1/2}(t+\Delta t))). \quad (A.1)$$

We now continuously deform $v_j(s) \equiv v(s) = sv_j + (1-s)\,v_{j+1}$, between $v_j = v(0)$ and $v_{j+1} = v(1)$, see (3.20a). With this in mind, the RHS of (A.1) becomes a function of the continuation parameter s, and $R_{j+1/2}(g)$ may be rewritten in the form

$$R_{j+1/2}(g) = \int_0^1 \frac{d}{ds}\,[\text{RHS}]\,ds. \quad (A.2)$$

From (3.2a) we may find the dependence of $v_{j+1/2}(t+\Delta t)$ on the continuation parameter s (for simplicity we omit the explicit dependence on time):

$$v_{j+1/2}(s) = \tfrac{1}{2}\left[v(s) + v_{j+1}\right] - \lambda[g_{j+1} - g(v(s))], \quad (A.3)$$

which in view of

$$\frac{d}{ds}v(s) = -\Delta v_{j+1/2}, \quad (A.4)$$

yields

$$\frac{d}{ds}U(v_{j+1/2}(s)) = -U'(v_{j+1/2}(s))\left[\frac{1}{2} + \lambda g'(v(s))\right] \cdot \Delta v_{j+1/2}. \quad (A.5)$$

In a similar manner, we have

$$\frac{d}{ds}U(v(s)) = -U'(v(s)) \cdot \Delta v_{j+1/2}, \quad (A.6)$$

and Leibnitz rule gives us

$$\frac{d}{ds}\left[-\lambda \int_{v(s)}^{v_{j+1}} U'(v)g'(v)\,dv\right] = -\lambda U'(v(s))\, g'(v(s)) \cdot \Delta v_{j+1/2}. \qquad (A.7)$$

Substitution of (A.5), (A.6), and (A.7) into (A.2) yields

$$R_{j+1/2}(g) = -\Delta v_{j+1/2} \int_0^1 \left[\frac{1}{2} + \lambda g'(v(s)\right] \cdot [U'(v(s)) - U'(v_{j+1/2}(s))]\, ds. \qquad (A.8)$$

Next, we use the continuation $v(r, s) = rv(s) + (1-r)\, v_{j+1}$ in (3.20b) in order to express the last difference on the right as

$$U'(v(s)) - U'(v_{j+1/2}(s)) = \int_0^1 \frac{d}{dr}\, U'(v_{j+1/2}(r, s))\, dr. \qquad (A.9)$$

This equality comes about as follows: in view of (3.20b), (3.2a), $v_{j+1/2}(r, s)$ is given by

$$v_{j+1/2}(r, s) = \tfrac{1}{2}[v(s) + v(r, s)] - \lambda[g(v((r, s)) - g(v(s))]; \qquad (A.10)$$

hence, $v_{j+1/2}(1, s) = v(s)$, $v_{j+1/2}(0, s) = v_{j+1/2}(s)$ and (A.9) follows.
    Noting that

$$\frac{d}{dr}\, v(r, s) = -\Delta v_{j+1/2} \cdot s, \qquad (A.11)$$

then by carrying out the differentiation on the RHS of (A.9), we obtain

$$\frac{d}{dr}\, U'(v_{j+1/2}(r, s)) = -U''(v_{j+1/2}(r, s)) \cdot \left[\frac{1}{2} - \lambda g'(v(r, s))\right] \cdot s\Delta v_{j+1/2}. \qquad (A.12)$$

Substituting (A.9), (A.11), and (A.12) into (A.8), we will end up with the desired identity (3.22). ∎

We close this section with the proof of Lemma 3.6. The piecewise linear interpolant of the grid function, $\{g_j\}$, chosen in (3.24),

$$g(v) = \frac{\Delta g_{j+1/2}}{\Delta v_{j+1/2}}\, (v - v_j) + g_j \qquad (A.13)$$

has a fixed slope at each cell:

$$g'(v(r, s)) = g'(v(s)) = \frac{\Delta g_{j+1/2}}{\Delta v_{j+1/2}}. \qquad (A.14)$$

From (A.14) and (3.22) we obtain that, in the case of quadratic entropy function where $U'' \equiv 1$,

$$R_{j+1/2}(g) = \frac{1}{2}(\Delta v_{j+1/2})^2 \left[\frac{1}{4} - \left(\lambda \frac{\Delta g_{j+1/2}}{\Delta v_{j+1/2}}\right)^2\right]. \qquad (A.15)$$

Moreover, the difference $g(v) - f(v)$ between two neighbouring values v_j and v_{j+1}, covers an area of size

$$\lambda \int_{v_j}^{v_{j+1}} (g(v) - f(v))\, dv = \frac{\lambda}{2} [g_{j+1} + g_j]\, \Delta v_{j+1/2} - \lambda \int_{v_j}^{v_{j-1}} f(v)\, dv. \quad (A.16)$$

Thus, in view of (A.15) and (A.16), the desired inequality, (3.26), boils down to

$$\frac{\lambda}{2} [g_{j+1} + g_j] \cdot \Delta v_{j+1/2} - \lambda \int_{v_j}^{v_{j+1}} f(v)\, dv + \frac{1}{2} \left(\lambda \frac{\Delta g_{j+1/2}}{\Delta v_{j+1/2}} \right)^2 - \frac{1}{8} (\Delta v_{j+1/2})^2 \leqslant 0. \quad (A.17)$$

To verify the inequality (A.17), we recall that by (3.2a), (3.2b) we have

$$g_m = f\left(v_m\left(t + \frac{\Delta t}{2} \right) \right) + \frac{1}{8\lambda} v'_m = f\left(v_m(t) - \frac{\lambda}{2} f'_m \right) + \frac{1}{8\lambda} v'_m, \qquad m = j, j+1, \quad (A.18)$$

and Taylor's expansion yields

$$g_m = f_m + \frac{1}{8\lambda} v'_m (1 - 4\beta^2) + O(\Delta v_{j+1/2})^2, \qquad \beta \equiv \lambda a(v_{j+1/2}(t)). \quad (A.19)$$

This enables us to write the first two terms on the left of (A.17) as

$$\frac{\lambda}{2} [g_{j+1} + g_j] \cdot \Delta v_{j+1/2} - \lambda \int_{v_j}^{v_{j+1}} f(v)\, dv$$

$$= \frac{1}{8} (1 - 4\beta^2) \cdot \left(\frac{v'_{j+1} + v'_j}{2\Delta v_{j+1/2}} \right) \cdot (\Delta v_{j+1/2})^2 + O(\Delta v_{j+1/2})^3. \quad (A.20)$$

Consider now the third term on the left of (A.17): by (A.19) we have

$$\lambda \Delta g_{j+1/2} = \lambda \Delta f_{j+1/2} + \frac{1}{8} (1 - 4\beta^2) \cdot \left(\frac{\Delta v'_{j+1/2}}{\Delta v_{j+1/2}} \right) \cdot \Delta v_{j+1/2}; \quad (A.21a)$$

inserting $\lambda \Delta f_{j+1/2} = \beta \Delta v_{j+1/2} + O(\Delta v_{j+1/2})^2$ into (A.21a), squaring the result, and rearranging, we obtain

$$\frac{1}{2} (\lambda \Delta g_{j+1/2})^2 = \frac{\beta^2}{2} (\Delta v_{j+1/2})^2 + \frac{\beta}{8} (1 - 4\beta^2) \cdot \left(\frac{\Delta v'_{j+1/2}}{\Delta v_{j+1/2}} \right) \cdot (\Delta v_{j+1/2})^2$$

$$+ \frac{1}{128} (1 - 4\beta^2)^2 \cdot \left(\frac{\Delta v'_{j+1/2}}{\Delta v_{j+1/2}} \right)^2 \cdot (\Delta v_{j+1/2})^2 + O(\Delta v_{j+1/2})^3. \quad (A.21b)$$

We note that the cubic term on the right of (A.20), (A.21b), consists of the error in the trapezodial rule

$$\frac{\lambda}{2} [f(v_{j+1}) + f(v_j)] \Delta v_{j+1/2} - \lambda \int_{v_j}^{v_{j+1}} f(v)\, dv = \frac{\lambda}{12} f''(v(\bar{x})) \cdot (\Delta v_{j+1/2})^3,$$

as well as additional contributions which are of the same order of magnitude

$$O(\Delta v_{j+1/2})^3 < \lambda \cdot [f''(v(\bar{x}))] \cdot (\Delta v_{j+1/2})^3. \tag{A.22}$$

Inserting (A.20), (A.21b), and (A.22) into the inequality (A.17) gives us

$$\frac{1-4\beta^2}{8}(\Delta v_{j+1/2})^2 \cdot \left[\frac{v'_{j+1}+v'_j}{2\Delta v_{j+1/2}} - 1 + \beta \frac{\Delta v'_{j+1/2}}{\Delta v_{j+1/2}} + \frac{1-4\beta^2}{16}\left(\frac{\Delta v'_{j+1/2}}{\Delta v_{j+1/2}}\right)^2 \right]$$
$$+ \lambda \cdot \max_x [f''(v(x))] \cdot (\Delta v_{j+1/2})^3 \leqslant 0. \tag{A.23}$$

The expression inside the left brackets can be upper bounded by

$$\left[\cdots \right] \leqslant \left[\left(\frac{v'_{j+1}+v'_j}{2\Delta v_{j+1/2}} + \left| \frac{v'_{j+1}-v'_j}{2\Delta v_{j+1/2}} \right| \right) - 1 \right.$$
$$\left. + \left(\beta - \frac{1}{2} \right) \left| \frac{\Delta v'_{j+1/2}}{\Delta v_{j+1/2}} \right| + \frac{1-4\beta^2}{16}\left(\frac{\Delta v'_{j+1/2}}{\Delta v_{j+1/2}}\right)^2 \right]. \tag{A.24}$$

By the CFL limitation, $\beta < \frac{1}{2}$, the sum of the last two terms is nonpositive, and since v'_j and v'_{j+1} agree in sign with $\Delta v_{j+1/2}$, we are left with the inequality

$$\left[\max\left(\frac{v'_j}{\Delta v_{j+1/2}}, \frac{v'_{j+1}}{\Delta v_{j+1/2}} \right) - 1 \right] + \lambda \cdot \max_x [f''(v(x))] \cdot \Delta v_{j+1/2} \leqslant 0,$$

which is met by the choice of entropy satisfying limiter in (3.25a), (3.25b).

REFERENCES

1. M. BEN-ARZI AND J. FALCOVITZ, *SIAM J. Sci. Stat. Comput.* **7**, No. 3 (1986).
2. R. J. DIPERNA, *Arch. Rat. Mech. Anal.* **82**, 27 (1983).
3. P. DUTT, ICASE Report No. 86-3, January 1986.
4. S. K. GODUNOV, *Mat. Sb.* **47**, 271 (1959). [Russian]
5. A. HARTEN, Ph.D. thesis, Research Develop. Report COU-3077.50, Courant Institute, N.Y.U., June 1974 (unpublished).
6. A. HARTEN, *Math. Comput.* **32**, 363 (1978).
7. A. HARTEN, *J. Comput. Phys.* **49**, 357 (1983).
8. A. HARTEN, ICASE Report No. 87-56, August 1987; *J. Comput. Phys.* **83**, 148 (1989).
9. A. HARTEN, B. ENGQUIST, S. OSHER, AND S. R. CHAKRAVARTHY, *J. Comput. Phys.* **71**, 231 (1987).
10. A. HARTEN, J. M. HYMAN, AND P. D. LAX, *Commun. Pure Appl. Math.* **29**, 297 (1976).
11. A. HARTEN AND P. D. LAX, *SIAM J. Num. Anal.* **18**, 289 (1981).
12. A. HARTEN AND S. OSHER, *SIAM J. Num. Anal.* **24**, 279 (1987).
13. P. D. LAX, *Commun. Pure Applied Math.* **7**, 159 (1954).
14. P. D. LAX, in *Contributions to Nonlinear Function Analysis*, edited by E. A. Zarantonello (Academic Press, New York, 1971), Vol. 31, p. 611.
15. P. D. LAX, *Hyperbolic Systems of Conservation Laws and the Mathematical Theory of Shock Waves*, Regional Conf. Series in Appl. Math. (SIAM, Philadelphia, 1973).
16. H. NESSYAHU, M.Sc. thesis, Tel-Aviv University, 1987 (unpublished).

17. S. OSHER, *SIAM J. Num. Anal.* **21**, 217 (1984).
18. S. OSHER AND E. TADMOR, *Math. Comput.* **50**, 19 (1988).
19. P. L. ROE, *J. Comput. Phys.* **43**, 357 (1981).
20. J. SMOLLER, *Shock Waves and Reaction-Diffusion Equations* (Springer-Verlag, New York, 1983).
21. G. A. SOD, *J. Comput. Phys.* **27**, 1 (1978).
22. E. TADMOR, *Math. Comput.* **43**, 353 (1984).
23. E. TADMOR, *Math. Comput.* **43**, 369 (1984).
24. B. VAN LEER, *J. Comput. Phys.* **32**, 101 (1979).
25. P. WOODWARD AND P. COLLELLA, *J. Comput. Phys.* **54**, 115 (1984).